

**GASTROINTESTINAL, HEPATOBILIARY, AND PANCREATIC PATHOLOGY**

# Loss of Hepatic Leucine-Rich Repeat-Containing G-Protein Coupled Receptors 4 and 5 Promotes Nonalcoholic Fatty Liver Disease



Enrica Saponara,\* Carlos Penno,\* Vanessa Orsini,\* Zhong-Yi Wang,\* Audrey Fischer,\* Alexandra Aebi,\* Meztli L. Matadamas-Guzman,<sup>†</sup> Virginie Brun,\* Benoit Fischer,\* Margaret Brousseau,<sup>‡</sup> Peter O'Donnell,<sup>‡</sup> Jonathan Turner,\* Alexandra Graff Meyer,<sup>§</sup> Laura Bollepalli,\* Giovanni d'Ario,\* Guglielmo Roma,\* Walter Carbone,\* Stefano Annunziato,\* Michael Obrecht,\* Nicolau Beckmann,\* Chandra Saravanan,<sup>‡</sup> Arnaud Osmont,\* Philipp Tropberger,\* Shola M. Richards,\* Christel Genoud,<sup>¶</sup> Svenja Ley,\* Iwona Ksiazek,\* Florian Nigsch,\* Luigi M. Terracciano,<sup>||</sup>\* Heiko S. Schadt,\* Tewis Bouwmeester,\* Jan S. Tchorz,\* and Heinz Ruffner\*

From the Novartis Institutes for BioMedical Research,\* Novartis Pharma AG, Basel, Switzerland; the Instituto Nacional de Medicina Genómica—Universidad Nacional Autónoma de México,<sup>†</sup> Mexico City, Mexico; the Novartis Institutes for BioMedical Research,<sup>‡</sup> Novartis Pharma AG, Cambridge, Massachusetts; the Friedrich Miescher Institute for BioMedical Research,<sup>§</sup> Facility for Advanced Imaging and Microscopy, Basel, Switzerland; the Electron Microscopy Facility,<sup>¶</sup> University of Lausanne, Lausanne, Switzerland; the Department of Biomedical Sciences,<sup>||</sup> Humanitas University, Pieve Emanuele, Milan, Italy; and the Istituto di Ricovero e Cura a Carattere Scientifico, Humanitas Research Hospital, Anatomia Patologica,\*\* Rozzano, Milan, Italy

Accepted for publication  
October 19, 2022.

Address correspondence to  
Heinz Ruffner, Ph.D., Novartis  
Institutes for BioMedical  
Research, Fabrikstr. 22-4.025.1,  
CH-4056 Basel, Switzerland.  
E-mail: [heinz.ruffner@novartis.com](mailto:heinz.ruffner@novartis.com).

The roof plate-specific spondin—leucine-rich repeat-containing G-protein coupled receptor 4/5 (LGR4/5)—zinc and ring finger 3 (ZNRF3)/ring finger protein 43 (RNF43) module is a master regulator of hepatic Wnt/ $\beta$ -catenin signaling and metabolic zonation. However, its impact on nonalcoholic fatty liver disease (NAFLD) remains unclear. The current study investigated whether hepatic epithelial cell-specific loss of the Wnt/ $\beta$ -catenin modulator Lgr4/5 promoted NAFLD. The 3- and 6-month-old mice with hepatic epithelial cell-specific deletion of both receptors Lgr4/5 (Lgr4/5dLKO) were compared with control mice fed with normal diet (ND) or high-fat diet (HFD). Six-month-old HFD-fed Lgr4/5dLKO mice developed hepatic steatosis and fibrosis but the control mice did not. Serum cholesterol—high-density lipoprotein and total cholesterol levels in 3- and 6-month-old HFD-fed Lgr4/5dLKO mice were decreased compared with those in control mice. An *ex vivo* primary hepatocyte culture assay and a comprehensive bile acid (BA) characterization in liver, plasma, bile, and feces demonstrated that ND-fed Lgr4/5dLKO mice had impaired BA secretion, predisposing them to develop cholestatic characteristics. Lipidome and RNA-sequencing analyses demonstrated severe alterations in several lipid species and pathways controlling lipid metabolism in the livers of Lgr4/5dLKO mice. In conclusion, loss of hepatic Wnt/ $\beta$ -catenin activity by Lgr4/5 deletion led to loss of BA secretion, cholestatic features, altered lipid homeostasis, and deregulation of lipoprotein pathways. Both BA and intrinsic lipid alterations contributed to the onset of NAFLD. (*Am J Pathol* 2023, 193: 161–181; <https://doi.org/10.1016/j.ajpath.2022.10.008>)

The liver consists of repetitive hexagonal structures called lobules. Hepatocytes in each lobule are divided into three types: periportal (zone 1), midzonal (zone 2), and pericentral (zone 3) hepatocytes. Liver function critically depends on complementary metabolic tasks distributed amongst hepatocytes alongside the portocentral blood flow. Examples of the spatial segregation of opposing metabolic tasks are the oxidative breakdown of fatty acids (FAs) (zone 1) and lipid

biosynthesis (zone 3), or gluconeogenesis (zone 1) and glycolysis (zone 3). Disruption of metabolic liver zonation

Supported by the Novartis Institutes for BioMedical Research Postdoctoral Program (E.S.).

Disclosures: All authors, except M.L.M.-G., A.G.M., C.G., and L.M.T., are or were employees of Novartis Pharma AG.

is therefore implicated in several metabolic disorders, such as diabetes and nonalcoholic fatty liver disease (NAFLD).<sup>1,2</sup>

NAFLD comprises a spectrum of liver conditions, including simple steatosis, nonalcoholic steatohepatitis (NASH), fibrosis, and cirrhosis, progressively leading to end-stage liver disease or hepatocellular carcinoma. Despite great progress in understanding the complexity of NAFLD, the understanding of the etiology and the pathophysiological mechanisms implicated in liver damage remains incomplete. One of the earliest hallmarks of NAFLD is the intrahepatic accumulation of neutral lipids concomitant with the alteration of lipid concentration in serum, a phenomenon known as dyslipidemia.<sup>3</sup> This imbalance is often attributable to altered hepatic lipid or bile acid (BA) synthesis, import or export, or alterations in intracellular cholesterol biosynthesis.<sup>4,5</sup> However, the instructive cues for these processes are not fully understood.

A centroportal Wnt/ $\beta$ -catenin activity gradient has been demonstrated to establish and maintain metabolic liver zonation. Moreover, increasing evidence suggests that Wnt/ $\beta$ -catenin signaling plays a role in both exogenous and endogenous lipid trafficking, regulates the expression of BA biosynthesis enzymes in hepatocytes,<sup>6,7</sup> and is required for proper bile canaliculi morphogenesis.<sup>8,9</sup> When Wnt ligands bind their cognate Frizzled receptor and the low density lipoprotein receptor-related protein 5/6 (LRP5/6) coreceptor, phosphorylation of LRP5/6 stabilizes  $\beta$ -catenin by decreasing the activity of the  $\beta$ -catenin destruction complex. Stabilized  $\beta$ -catenin accumulates in the cytoplasm and can now enter the nucleus, where it binds to T-cell factor (TCF) family transcription factors and enhances the transcription of  $\beta$ -catenin target genes,<sup>10</sup> including many pericentral metabolic enzymes, such as cytochrome P450 family 2 subfamily E member 1 (Cyp2e1) and Cyp2a1, or the tight junction (TJ) protein Claudin-2 (CLDN2).<sup>11</sup> Consequently, loss of Wnt/ $\beta$ -catenin signaling abrogates the expression of pericentral metabolic genes while increasing periportal metabolic genes, whereas pathway activation caused the opposite phenotype.<sup>12–14</sup> Roof plate-specific spondin (Rspo) 1–4 ligands potentiate Wnt/ $\beta$ -catenin signaling following binding to their receptors Lgr4–6. This is achieved by clearing the cell-surface transmembrane E3 ubiquitin ligases zinc and ring finger 3 (Znrf3) and its homologue ring finger protein 43 (Rnf43), which promote WNT receptor turnover at the plasma membrane.<sup>15–18</sup> Complete loss of hepatic Wnt/ $\beta$ -catenin signaling in mice with hepatic epithelial cell-specific deletion<sup>19</sup> of *Lgr4/5* showed that the Rspo-Lgr4/5-Znrf3/Rnf43 module is a critical regulator, rather than just a potentiator, of hepatic Wnt/ $\beta$ -catenin activity and metabolic zonation.<sup>20</sup> Moreover, combined deletion of *Znrf3/Rnf43* or Rspo injections expanded the pericentral metabolic program throughout the liver, reprogramming periportal into pericentral hepatocytes and thus disrupting metabolic liver zonation. However, the implication of the Rspo-Lgr4/5-Znrf3/Rnf43 module on NAFLD is unclear.

A recent report suggests that hepatocyte-specific loss of Znrf3/Rnf43 leads to steatohepatitis and imbalance in liver fat composition in normal diet (ND)—fed mice. The authors propose that the mutant mice exhibit altered hepatocyte regeneration that predisposes to hepatocellular carcinoma.<sup>21</sup> Hepatocyte-specific expression of an activated  $\beta$ -catenin transgene results in pronounced pericentral steatosis under high-fat diet (HFD) conditions, showing diet-induced obesity, systemic insulin resistance, and increased hepatic expression of glycolytic and lipogenic genes. However, animals fed with ND have normal liver histology and body weight.<sup>22</sup> In contrast, the combined deletion of Znrf3/Rnf43 and the resulting increase in Wnt/ $\beta$ -catenin signaling does not lead to the spontaneous development of NAFLD but promotes uncontrolled hepatocyte proliferation and tumor formation within an observation period of 1 year.<sup>23</sup> These findings are in line with previous work suggesting that liver-specific loss of Wnt/ $\beta$ -catenin signaling, rather than its increase, leads to NAFLD and NASH.<sup>22,24,25</sup>

To clarify the controversial role of the Rspo-LGR4/5-ZNRF3/RNF43 module in NAFLD, the current study investigated lipid metabolism and NAFLD in mice with hepatic epithelial cell-specific deletion of *Lgr4/5*. The results were in agreement with, and expanded on, the information published in Saponara et al.<sup>26</sup> Mice of different age were analyzed for steatotic and fibrotic manifestation under ND and HFD conditions, and *ex vivo* hepatocyte cultures from the knockout (KO) and control mice were utilized to study lipid uptake and storage and BA secretion. The results demonstrated that loss of Wnt/ $\beta$ -catenin signaling on deletion of *Lgr4/5* in mouse hepatic epithelial cells led to a NASH-like phenotype characterized by steatosis and fibrosis on HFD. Several lipid species were increased in livers of KO mice, and serum lipids were decreased.

## Materials and Methods

### Mouse Model Generation and Animal Experimentation

Hepatic epithelial cell-specific deletion of both *Lgr4* and *Lgr5* receptors was achieved, as previously described.<sup>19,20</sup> Briefly, mouse models for conditional KO of both *Lgr4* (*Lgr4lox*) and *Lgr5* (*Lgr5lox*) alleles were crossed with *Alb-Cre* mice (*Lgr4/5dLKO*). *Alb-Cre*—negative, *Lgr4/5<sup>fl/fl</sup>* mice were utilized as controls. Unless differently specified, both male and female animals were used in this study. HFD: For 3- and 6-month time points, mice were housed with ad libitum access to water and food until the age of 2 and 5 months, respectively. Afterwards, they were fed with HFD, 45% kcal (number 2126; Kliba/NAFAG, Kaiseraugst, Switzerland) for 4 consecutive weeks (1 month). Age-matched animals were maintained on ND. All animal experimentation was conducted in Basel, Switzerland, in accordance with the Swiss Animal Welfare Legislation, and authorized by the cantonal veterinary office of Basel. All mice had unrestricted access to water and food, and animal

experimentation was conducted in accordance with animal law of Basel-Stadt, Switzerland. The Novartis Campus animal facilities comprise a specific pathogen-free animal breeding facility and a clean facility for experimental surgery and physiology. Biosecurity and pathogen exclusions follow the Federation of European Laboratory Animal Science Associations health monitoring guidelines, and animals are screened quarterly. Mice were housed in Allentown XJ individually ventilated cages in a 12:12 light/dark cycle. Environmental enrichments included nestlets, wood sticks, and mouse houses.

### Primary Hepatocyte Purification, Long-Term Culture

Perfusion procedures were performed at 37°C, 7 mL/minute constant flow rate, with the Harvard mini-peristaltic pump. Livers were initially cleared from blood utilizing 35 to 50 mL/mouse of preperfusion solution consisting of 1× Hanks' balanced salt solution (HBSS) without Ca<sup>2+</sup>, Mg<sup>2+</sup>, 0.5 mmol/L EGTA, and 10 mmol/L HEPES. After 5 minutes, the preperfusion solution was substituted with perfusion solution: Dulbecco's modified Eagle's medium/F12, 3 mmol/L CaCl<sub>2</sub>, penicillin-streptomycin, 20 mmol/L HEPES, and collagenase (120 collagenase digestive units/mL; Roche Diagnostics, Rotkreuz, Switzerland; number 11088793001). The liver was perfused for the next 10 minutes, removed from the abdominal cavity, and placed into a 10-cm dish with ice-cold wash solution (Dulbecco's modified Eagle's medium/F12 supplemented with penicillin-streptomycin and 10% fetal bovine serum). Liver lobes were torn apart with forceps, and hepatic cells were released into wash solution.

Cells were collected and 2× washed in wash solution by centrifugation at 50 × *g* for 5 minutes, 4°C, then suspended in attachment media consisting of Williams E medium without phenol red, penicillin-streptomycin, 10% fetal bovine serum, 1:10,000 insulin (1.7 mmol/L), Glutamax, 0.3 mmol/L dexamethasone, and 10 mmol/L HEPES. Cells were further purified on a 21.6 mL Percoll (GE Healthcare, Chicago, IL; number 17-0891-02) gradient supplemented with 2.4 mL of 10× Hanks' balanced salt solution and finally washed 2× in 25 mL attachment medium by centrifugation at 60 × *g* for 3 minutes, 4°C. A total of 220,000 cells/well were distributed on 24-well collagen 1-coated plates [Becton Dickinson (BD), Allschwil, Switzerland; number 356408] and incubated at 37°C, 5% CO<sub>2</sub>. The basal media utilized in all conditions consisted of Williams E medium (Sigma, St. Louis, MO; number W1878), penicillin-streptomycin, 1:10,000 insulin (1.7 mmol/L), Glutamax, 1:10,000 dexamethasone (0.3 mmol/L), and 10 mmol/L HEPES.

### Ex Vivo Hepatocyte Assays

LDL-Phrodo assay: Primary hepatocytes were kept overnight in basal medium. On the following day, LDL-Phrodo

red (Life Technologies, Carlsbad, CA; number I34360) was added to each well at the final concentration of 10 µg/mL. Imaging and OD were acquired after 5, 10, 15, 20, and 24 hours with Arrayscan XTI (Cellomics, Thermo Fisher Scientific, Pittsburgh, PA). After the final measurement, cells were washed with phosphate-buffered saline and incubated 1 minute with BODIPY FL working solution at 20 µg/mL together with the nuclear dye Hoechst.

### CLF Assay

After seeding, cells were incubated in attachment medium for 4 hours. Afterward, ice-cold Matrigel was added at a final concentration of 250 µg/mL. Cells were cultured over a period of 7 days in basal medium. Matrigel was renewed every second day. At day 7, cells were incubated for 25 minutes at 37°C with cholesteryl-L-lysyl-fluorescein (CLF; Corning, Reinach, Switzerland) at a final concentration of 5 mmol/L. CLF-positive canaliculi were imaged utilizing Arrayscan XTI.

### Lipid Droplet Analysis

After isolation, cells were cultured in basal media over 24 hours. Cells were fixed with 10% paraformaldehyde and afterward stained with BODIPY FL. Lipid droplet-size quantification was performed with the cell imaging software Imaris x64 version 7.6.5 (Oxford Instruments, Abingdon, UK).

### Blood Sample Preparation

After each experiment, animals were euthanized with CO<sub>2</sub>, and blood was collected from the vena cava. Serum was obtained by centrifuging blood at 10,000 × *g* for 90 seconds into a Microtainer Tube, 400 to 600 µL, SST Gel Serum Separator Additive, Clear (BD; number 365967), and kept at −20°C until further processing.

### Glucose and Insulin Tolerance Tests

Mice were fasted for 17 and 6 hours, respectively, and baseline blood glucose levels were measured in tail-vein blood using an Accu-Chek Compact plus glucometer (Roche Diagnostics). Glucose (3 g/kg body weight) or insulin (0.75 U/kg body weight) was injected intraperitoneally. Blood glucose levels were measured before and at 15, 30, 45, 60, 90, and 120 minutes after glucose or insulin injection, as previously described.<sup>27</sup>

### FPLC-Based Size Exclusion

A total of 50 to 100 µL of serum per samples was pooled and utilized for fast protein liquid chromatography (FPLC) measurement. FPLC was conducted using a BioLogic DuoFlow FPLC System - Two Column (BioRad, Hercules, CA), Superose 6 Increase, 10/300GL, FPLC column (GE Healthcare; number 29-0915-96), BioLogic BioFrac

Fraction Collector (BioRad), and blood bank saline. To measure total cholesterol and triglycerides (TGs), these reagents were used: SpectraMax M2 Spectrophotometer (Molecular Devices, San Jose, CA), Total Cholesterol Kit (Wako Diagnostics, Mountain View, CA; Cholesterol E), L-Type Triglyceride M (Wako Diagnostics; Enzyme Color R1 and R2), and a 96-well, half-area plate (Corning, Teterboro, NJ; number 3690).

### TG Secretion *in Vivo*

The triglyceride secretion assay was conducted in the Association for Assessment and Accreditation of Laboratory Animal Care—accredited Novartis Institutes for BioMedical Research Basel vivarium under license BS-2116. ND-fed Lgr4/5dLKO (four females and five males) and control mice (eight females and seven males), aged 9 to 15 weeks at study start, were enrolled in the TG secretion assay. Mice were fasted for 10 hours before the start of the triglyceride secretion assay. An injectable poloxamer-407 solution (Pluronic F-127; Sigma-Aldrich Merck, Darmstadt, Germany) was prepared with prechilled Dulbecco's phosphate-buffered saline (Gibco, Thermo Fisher Scientific, Reinach, Switzerland) at a final concentration of 100 mg/mL. The solution was incubated overnight at 4°C under vigorous stirring. All the mice were given 1 g/kg body weight poloxamer-407 (10 mL/kg; intraperitoneally). Blood was sampled 5 minutes before (baseline) and 60, 120, and 180 minutes after treatment from the saphenous vein in a CB300Z microvette (Sarstedt), as well as at 240 minutes via cardiac puncture in a 1.1-mL Z gel monovette (Sarstedt, Nümbrecht, Germany). After a minimum coagulation time of 30 minutes, serum was obtained by centrifugation at room temperature and 2000 × *g* for 10 minutes and stored in low-bind Eppendorf tubes at −80°C. For analysis, serum samples were diluted 1:15 with standard diluent assay buffer before assaying, and serum triglyceride levels were measured using an enzyme-linked immunosorbent enzymatic assay (Triglycerides Colorimetric assay kit; number 10010303; Cayman Chemical, Ann Arbor, MI) in a microplate reader (Gen 5; Biotek, Winooski, VT).

### Immunohistochemistry

Formalin-fixed, paraffin-embedded mouse liver sections (3 μm thick) were stained by hematoxylin and eosin and picosirius red using standard protocols. The following primary antibodies were used for immunohistochemistry and immunofluorescence analyses: mouse anti-cadherin 1 antibody clone 36 (BD; number 610181), anti-ionized calcium-binding adapter molecule 1 (Abcam, Cambridge, UK; number ab178846), rat anti-keratin 19 (KRT19) [Developmental Studies Hybridoma Bank, #TROMA-III; University of Iowa, Iowa City, IA; Research Resource Identifier: AB\_2133570], and rabbit anti- $\alpha$ -smooth muscle

actin antibody (EPR5368) (Abcam; number ab124964). OCT-embedded tissue (7 μm thick) or primary hepatocytes were stained by BODIPY FL (Life Technologies; number D2184) and rabbit anti-zona occludens protein-1 (Invitrogen, Waltham, MA; number 617300). Digital images were acquired with the Aperio ScanScope XT system (Leica Biosystems, Wetzlar, Germany) or with a Zeiss LSM 700 (Zeiss, Jena, Germany) confocal microscope using the Zen 2011 SP3 (black edition) software (Zeiss, Feldbach, Switzerland). Automated image analysis was done using the HALO system software version 3.3.2541.262 (Indica Labs, Albuquerque, NM). Lipid droplet size quantification was performed with the cell imaging software Imaris x64 version 7.6.5 (Oxford Instruments). For picosirius red,  $\alpha$ -smooth muscle actin ( $\alpha$ -SMA), and ionized calcium-binding adapter molecule 1 (IBA1) staining, the positive signal was measured using a color deconvolution algorithm with a classifier to exclude vessels. To quantify steatosis on hematoxylin and eosin-stained slides, a vacuole module count from Indica laboratory with a classifier to exclude vessels was used.

### IL-6 and TNF- $\alpha$ Homogeneous Time Resolved Fluorescence Assays

IL-6 and tumor necrosis factor (TNF)- $\alpha$  were measured in sera of mice utilizing the mouse IL-6 assay (number 62MIL06-PEG) and mouse TNF- $\alpha$  assay (number 62CTNFAPEG), according to Cisbio Bioassays (Codolet, France) vendor protocols.

### RNA Isolation and Library Preparation

Total RNA was isolated from mouse livers with Qiazol (Invitrogen; number 79306) and purified with the miR-Neasy kit (Qiagen, Basel, Switzerland; number 217004). The amount of RNA was quantified with the Agilent RNA 6000 Nano Kit (Agilent Technologies, Santa Clara, CA; number 5067-1511). RNA-sequencing libraries were prepared from mouse liver total RNA using the Illumina (San Diego, CA) TruSeq Stranded Total RNA sample preparation protocol, following the manufacturer's instructions.

### RNA Sequencing

RNA sequencing and related data analysis were performed as described by Planas-Paz et al.<sup>20</sup> Differential expression among Lgr4/5dLKO and control mice was visualized as volcano plots with the TIBCO Spotfire software version 11.4.3 (Palo Alto, CA). RNA-sequencing raw data are available at the NIH Sequence Read Archive (identifier: PRJNA670351; <https://www.ncbi.nlm.nih.gov/sra/?term=PRJNA670351>, last accessed October 21, 2020).

## RNA Extraction, Reverse Transcription, and Quantitative PCR

Total liver RNA was isolated using the RNeasy mini kit, including on-column DNase digestion, according to the manufacturer's instructions (Qiagen). RNA from each tissue sample (2 µg) was reverse transcribed using the high-capacity cDNA reverse transcription kit (Applied Biosystems, Waltham, MA). The resulting cDNA products were diluted 1:20 and subjected to quantitative PCRs using TaqMan reagents. Quantitative PCRs were conducted on an ABI Prism 7900HT Sequence Detection System (Applied Biosystems). The threshold cycle value ( $C_T$ ) was determined for each transcript and normalized to the internal control transcript glyceraldehyde-3-phosphate dehydrogenase. The relative quantification of each mRNA species was assessed using the comparative  $C_T$  method. Statistical analysis was performed using the *t*-test with the GraphPad Prism software version 8.1.2 (GraphPad Software, San Diego, CA). Primers utilized in this study were cadherin 1 (Cdh1), Mm01247357\_m1;  $\beta$ -catenin (Ctnnb1), Mm00483039\_m1; and axis inhibition protein 2 (Axin2), Mm00443610\_m1.

## In Situ Hybridization

Sections (5 µm thick) from human normal control, non-alcoholic steatohepatitis, and cirrhotic formalin-fixed, paraffin-embedded samples (Novartis tissue archive) were processed using the RNAscope 2.0 Detection Kit, according to the manufacturer's instructions (Advanced Cell Diagnostics, Hayward, CA). RNAscope probes used were human *LGR4* (number 460559) and *LGR5* (number 311029), positive control probe *PP1B* (a housekeeping gene; number 313906-C2), and *DapB* (a bacterial gene) negative control probe (number 310048). The *in situ* hybridization method followed protocols established by ACDBio (Newark, CA) and Ventana Medical Systems (Tucson, AZ) with signal detection by horseradish peroxidase and hematoxylin counterstain. *In situ* hybridization signal in tissues was graded in a semiquantitative scale (from 0 to 4, where 0 indicates no evidence of staining) incorporating both number and distribution of specific staining.

## Pathway Enrichment Analysis for Differentially Expressed Genes

The clusterProfiler<sup>28</sup> and ReactomePA<sup>29</sup> R packages were used to perform Reactome pathway enrichment analysis for up-regulated and down-regulated genes in Lgr4/5dLKO mice. The Fisher exact test, followed by the Benjamini-Hochberg correction, was performed for statistical analysis, and an adjusted  $P < 0.05$  was set as the cutoff criterion. A gene was declared differentially expressed if a difference observed in expression between two experimental conditions was statistically significant (adjusted  $P < 0.05$ ).

$\log_2$  fold change of expression was used to define up-regulation or down-regulation.

## Identifying Overrepresented Transcription Factor Motifs in Gene Lists

The R package RcisTarget was used to identify enriched transcription factor motifs associated with down-regulated genes in Lgr4/5dLKO mice, using the cisTarget v9 transcription factor motif annotations and the mm9 database of motif rankings.<sup>30</sup>

## Quantitative BA Profile Analysis in Plasma, Bile, Feces, and Liver by UPLC Tandem Mass Spectrometry

BA and 7 $\alpha$ -hydroxy-4-cholesten-3-one (C4) analyses were performed on an Agilent 1290 Infinity Ultra high-performance liquid chromatography (UPLC) system interfaced to an ABSciex (Framingham, MA) QTRAP6500 triple-quadrupole tandem mass spectrometer equipped with an electrospray ionization source [liquid chromatography–mass spectrometry (LC-MS)]. All data were acquired and analyzed using Analyst 1.7.1 data processing software (ABSciex). BAs and C4 were separated on an Acquity UPLC BEH C18, 1.7 µm, 2.1 × 150-mm (Waters, Milford, MA; number 186002353) analytical chromatography column maintained at 70°C at a flow rate of 0.5 mL/minute. The mobile phases consisted of (A) 95:5 (v/v) water/acetonitrile (water LC-MS grade; VWR International, Radnor, PA; number 83645.290; acetonitrile LC-MS Chromasolv; Merck, Darmstadt, Germany; number 100029) with formic acid (0.1%; VWR; number 84865.180) and (B) 5:95 (v/v) water/acetonitrile with formic acid (0.1%). A sample volume of 5 µL was used for injection into the LC-MS system. The separation was conducted under the following gradient: 0 minutes 10% (B); 0.5 minutes 10% (B); 3.5 minutes 20% (B); 15.2 minutes 33% (B); 22 minutes 65% (B); 23 minutes 100% (B); and 26 minutes 100% (B). Sample temperature was maintained at 8°C.

For plasma and liver analysis, calibration standards were prepared in aqueous 5% bovine serum albumin (Sigma-Aldrich, St. Louis, MO; number A6003-25g) solution. Approximately 250 mg of liver was fully homogenized in a solution of methanol/water 1:1 (v/v) using a Precellys Evolution Homogenizer (Bertin Technologies, Montigny-le-Bretonneux, France) to obtain homogenates containing 250 mg liver per mL. Plasma (50 µL), liver homogenates (100 µL), and calibration standards (50 µL for plasma, and 100 µL for liver) were spiked with internal standard solution (50 or 100 µL, respectively) containing analyte-matching stable isotope compounds in acetonitrile at concentrations of 200 nmol/L, each. Extraction of analytes was achieved by addition of acetonitrile to precipitate proteins (450 µL for plasma; 700 µL + 100 µL of water for liver homogenates), followed by centrifugation at 20,000 × *g* for ≥10 minutes. The clear supernatant was transferred into a new tube and evaporated to dryness. The dry residue was reconstituted in

methanol/water 1:1 (v/v) containing 0.1% formic acid (60  $\mu$ L for plasma, and 150  $\mu$ L for liver) and analyzed by LC-MS. For bile analysis, both calibration standards and samples (diluted 1:50,000) were prepared in methanol/water 1:1 (v/v) containing 0.1% formic acid, spiked with 50  $\mu$ L internal standard solution, and analyzed by LC-MS. For feces analysis, a multistep extraction procedure was applied according to a published protocol,<sup>31</sup> with modifications. Approximately 20 mg of fecal samples was accurately weighed in a 2-mL reaction tube after the empty tube weight had been recorded, followed by 1:10 (w/w) dilution in water (nominal 200  $\mu$ L). The sample was mixed, allowed to soak/swell for 5 minutes at room temperature, and mixed again to obtain a homogeneous slurry. After centrifugation at  $20,000 \times g$  for 8 minutes, the clear supernatant was transferred into a new tube, and the residual pellet was extracted with 400  $\mu$ L of methanol, followed by another centrifugation and extraction step with 400  $\mu$ L of acetonitrile. The clear supernatants from all extraction steps were combined, internal standard solution was added, and extracts were evaporated to dryness. The dry residue was reconstituted in 500  $\mu$ L methanol/water 1:1 (v/v) containing 0.1% formic acid and analyzed by LC-MS. Calibration standards were prepared out of solvent matching the solvent composition of the sample extracts and treated the same way as the samples.

### Lipid Extraction

Lipid extraction was done in 5 mg of liver resections. A volume of 800  $\mu$ L of chloroform/methanol (2:1 v/v) containing 15- $\mu$ L internal standards (EquiSPLASH; Avanti Polar Lipids, Birmingham, AL) was homogenized using the bead beating device (Precellys, Rockville, MD) maintained at 4°C. After homogenization, samples were mixed for 30 minutes at 4°C and centrifuged at  $17,500 \times g$  for 10 minutes at 4°C. Supernatants were collected, and 100  $\mu$ L of water was added to induce phase separation. Samples were gently mixed for 30 minutes at 4°C. The lower phase was collected and evaporated under nitrogen. Samples were reconstituted in 100  $\mu$ L of isopropanol. A pooled sample (quality control sample) was generated to assess analytical quality, and an extraction blank sample was generated to determine contaminant masses derived from reagents and materials.

### UPLC-Q Exactive Orbitrap/Mass Spectrometry–Based Untargeted Lipidomics Analysis

The LC system consisted of a Dionex Ultimate 3000 RS coupled with a HESI probe to a Q Exactive Orbitrap mass spectrometer (Thermo Fisher, Waltham, MA). Lipids were separated on an Accucore UPLC C30 column (150  $\times$  2.1 mm; 2.6  $\mu$ m) (Thermo Fisher). The column was maintained at 50°C at a flow rate of 0.3 mL/minute. The mobile phases consisted of (A) 60:40 (v/v) water/acetonitrile with ammonium formate (5 mmol/L) and formic acid (0.1%) and (B)

80:20 (v/v) isopropanol/acetonitrile with ammonium formate (5 mmol/L) and 0.1% formic acid. A sample volume of 5  $\mu$ L was used for the injection. The separation was conducted under the following gradient: 0 minutes 25% (B); 20 minutes 86% (B); 22 minutes 90% (B); 24 minutes 99% (B); 26 minutes 99% (B); and 32 minutes 25% (B). Sample temperature was maintained at 4°C. MS1 and MS/MS (data-dependent MS/MS) data in positive and negative ion modes were independently acquired. For the full MS, the automatic gain control target was set as  $1 \times 10^6$  and the maximum injection time was set as 250 milliseconds. In the data-dependent MS/MS, the automatic gain control target was set as  $1 \times 10^5$  and the maximum injection time was set as 120 milliseconds. The source parameters were as follows: in electrospray ionization(+): sheath gas pressure, 60; auxiliary gas flow, 3; spray voltage, 4.0 kV; capillary temperature, 400°C; in electrospray ionization(–): sheath gas pressure, 40; auxiliary gas flow, 2; spray voltage, 3.5 kV; capillary temperature, 450°C; auxiliary gas heater temperature, 390°C. MS1 mass range, m/z 200 to 1500; MS1 resolving power, 35,000 full width at half maximum (m/z 200); number of data-dependent scans per cycle, 10; and MS/MS resolving power, 17,500 full width at half maximum (m/z 200). The data-dependent MS/MS mode top *N* was 10; the normalized collision energy values were 15, 25, and 35 for both positive and negative; and the isolation window was m/z 1.0. The instrument was tuned using positive and negative ion mode calibration solutions (Thermo Fisher). The shorthand notation system and nomenclature of lipids used are the same as those used by Tsugawa et al.<sup>32</sup>

### Lipid Data Analysis and Lipid Identification

The raw format files were also converted to ABF format using an ABF converter. MS-DIAL 4.48 (lipidomics mode) was used for peak extraction, peak alignment, deconvolution analysis, and identification.<sup>32</sup> Parameter settings were as follows. Data collection: MS1/MS2 tolerance, 0.01/0.05 Da; and minimum peak height,  $5 \times 10^6$  and  $1 \times 10^6$  of amplitude for positive and negative ion mode, respectively. Identification: accurate mass tolerance MS1/MS2, 0.01/0.05 Da; and score cutoff, 90%. Alignment: retention time tolerance, 0.1 minutes; and MS1 tolerance, 0.01 Da. All lipid annotations produced with negative and positive acquisition were merged with in-house built scripts in R version 3.6.3 (<https://www.r-project.org>). Further data processing, including missing values imputation, logarithmic transformation (base 2), normalization (based on EquiSPLASH and scaling methods), and group comparisons (empirical Bayes-moderated *t*-tests), was performed in R version 3.5.3 with packages Metabolomics and NormalizeMets.<sup>33,34</sup> The nomenclature of lipid classes is described in MS-DIAL (<http://prime.psc.riken.jp/compms/>)

[msdial/lipidnomenclature.html](https://msdial.lipidnomenclature.html), last accessed April 21, 2021).

### Serum Biochemistry Analysis

Aspartate aminotransferase (AST), alanine aminotransferase (ALT), t-Chol, c-HDL, and TG were measured in sera of mice utilizing the Spotchem II Kenshin-2 kit (Axon Lab, Baden-Dättwil, Switzerland).

### Transmission Electron Microscopy

The mouse liver was cut into 2 to 3 mm<sup>3</sup> cubes and immediately immersed in a fixation solution containing 2.5% glutaraldehyde (Electron Microscopy Science, Hatfield, PA) in 0.1 mol/L cacodylate buffer (pH 7.4) for 1 hour at room temperature and then overnight at 4°C. After five washes in 0.1 mol/L cacodylate buffer (pH 7.4), a post-fixation in 1% osmium tetroxide in 0.1 mol/L cacodylate buffer (pH 7.4) was done. After five washes in double-distilled water and dehydration steps in a graded alcohol series, the mouse liver pieces were embedded in Embed 812 epoxy resin hard (Electron Microscopy Science) for 12 hours and polymerized at 60°C during 48 hours. For transmission electron microscopy analysis, a region of interest was selected under bright field. After trimming, silver/gray thin sections (50 nm thickness) were collected on formvar-coated single-slot copper grids (Electron Microscopy Science). After post-staining with 1% uranyl acetate and lead citrate (6 minutes, each), images were recorded using a FEI Tecnai Spirit (FEI Company, Eindhoven, the Netherlands) operated at 120 keV using a side-mounted 2000 × 2000 pixels charge-coupled device camera (Veleta; Olympus, Münster, Germany).

### Ultrasound Elastography

**Acquisition:** Animals were anesthetized using 2.0% isoflurane (Abbott, Cham, Switzerland) in 100% O<sub>2</sub> and placed on an electrical warming pad to maintain body temperature at 37°C throughout the assessment. The anesthesia was maintained during the image acquisition by delivering the anesthetic via a nose cone, and the eyes were protected with Viscotears Augen-Gel creme. The animals were positioned in a supine position. After shaving the abdomen, mice were fixed with tape on the upper and lower parts of the body. All examinations were performed according to a standardized protocol with an ultrasound system (Aixplorer; SuperSonic Imagine, Aix-En-Provence, France) equipped with a 25-MHz (SL25-15) superficial linear transducer. The transducer was fixed to a micromanipulator and positioned precisely in the transversal plane. The examination began with gray-scale B-mode to visualize sternum and liver underneath. Afterwards, three measurements in the shear wave elastography mode were made in three different places from sternum to stomach. Ultrasound gel (Aquasonic 100; Parker

Laboratories Inc., Fairfield, NJ) was placed between the skin and the ultrasound transducer. During the shear wave elastography assessment, care was taken not to put any pressure to the liver by the transducer. The liver elasticity (kPa) was measured in shear wave elastography mode by placing the region of interest at the thickest portion of the liver in each of the three slices measured (total 3 values, from which the mean stiffness was derived for each mouse).

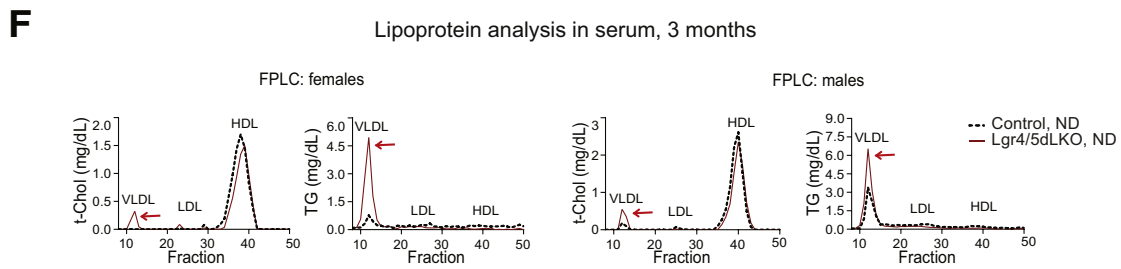
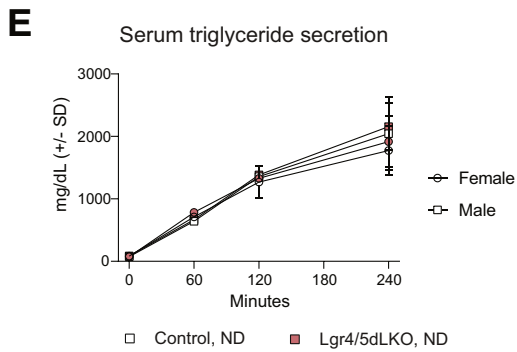
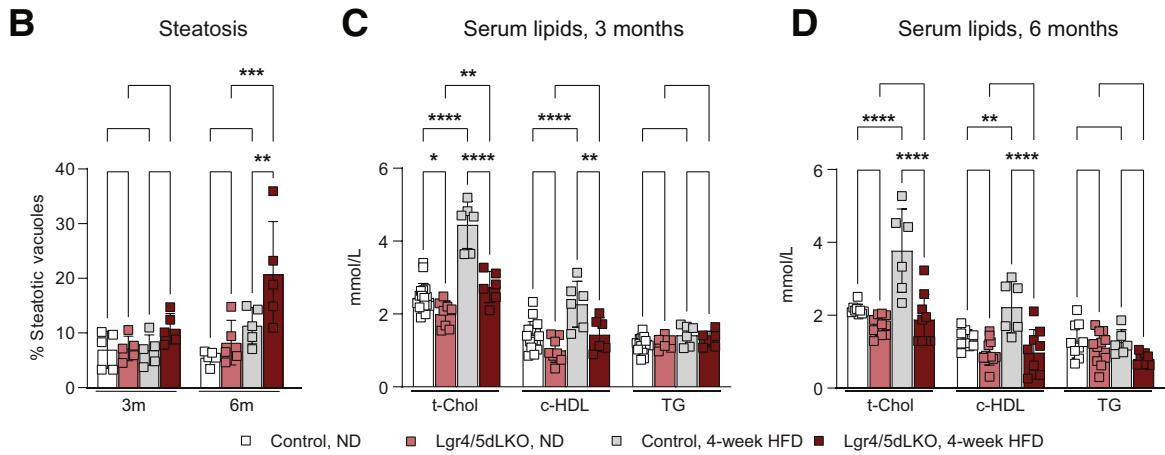
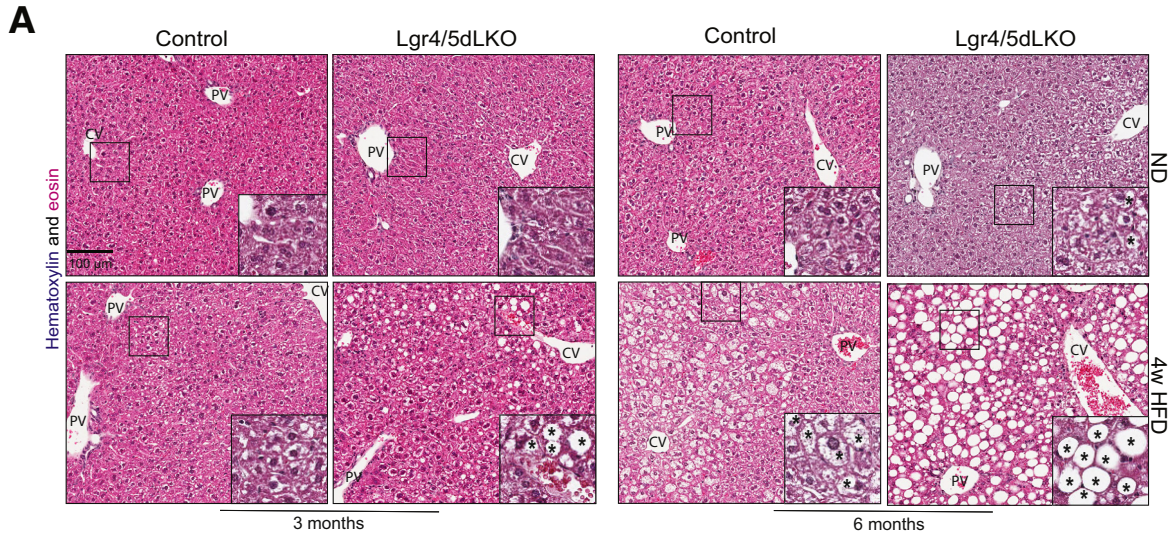
### Statistical Analysis

For analysis of serum biochemistry (ALT and AST), homogeneous time resolved fluorescence assays (IL-6 and TNF- $\alpha$ ), CLF assay, BODIPY FL quantification, and *Cdh1*, *Axin2*, and *Ctnnb1* gene expression between two groups, a two-tailed *t*-test was performed. For analysis of LDL-Phrodo uptake over time and serum levels of total cholesterol (t-Chol), cholesterol–high-density lipoprotein (c-HDL) and TG, a two-way analysis of variance was performed. *P* < 0.05 was considered significant, and plots display means  $\pm$  SD in case of biological replicates. All statistical analyses and graph generation were performed using the GraphPad Prism 8.1.2 software. For RNA-sequencing analysis, the method utilized is described by Planas-Paz et al.<sup>20</sup> Briefly, Limma R package from the Bioconductor suite (<https://www.bioconductor.org>) was used to identify genes differentially expressed between the conditions of interest. *P* values were adjusted for multiple hypotheses using the Benjamini-Hochberg correction. Genes were defined differentially expressed if *P*  $\leq$  0.01 with at least a twofold change in either direction.

## Results

### Lgr4/5dLKO Mice Display Hepatic Lipid Accumulation and Altered Serum Lipoprotein Levels

Mice with an albumin-Cre–mediated (*Alb-Cre*; *Lgr4/5<sup>fl/fl</sup>*) combined deletion of *Lgr4* and *Lgr5* in hepatocytes and biliary cells (*Lgr4/5dLKO*) exhibit compromised metabolic zonation and liver regeneration potential.<sup>20</sup> The current work focused on the consequences of loss of Wnt-dependent metabolic zonation in mouse livers. Specifically, the liver and serum phenotypes were investigated in *Lgr4/5dLKO* and control mice at 3 and 6 months of age, fed with either ND only (ND; denoted subsequently as 3- and 6-month–old ND-fed mice), or with ND for 2 and 5 months before a moderate obesogenic 45% kcal high-fat diet (HFD) challenge for 4 weeks, respectively (denoted subsequently as 3- and 6-month–old HFD-fed mice), before analysis (Supplemental Figure S1A). Livers of 3-month–old ND-fed *Lgr4/5dLKO* mice appeared histologically intact (Figure 1, A and B). Serum t-Chol was reduced in *Lgr4/5dLKO* compared with control (*Alb-Cre*–negative, *Lgr4/5<sup>fl/fl</sup>*) mice, whereas c-HDL and TG levels were similar (Figure 1C). t-Chol reduction was modest but significant, because mouse



serum t-Chol levels measured over a period of 20 weeks are rather stable.<sup>35</sup> The fact that TG levels were similar in the two strains was suggestive of a latent dyslipidemia in Lgr4/5dLKO animals. No abnormality concerning glucose or insulin tolerance was detected in 3-month-old ND-fed Lgr4/5dLKO mice (Supplemental Figure S1B). Under HFD conditions, the 3-month-old Lgr4/5dLKO mice developed mild and scattered liver steatotic foci in contrast to control animals, without reaching statistical significance (Figure 1, A and B). However, the Lgr4/5dLKO mice showed a marked reduction in serum t-Chol and c-HDL levels compared with control animals on HFD, whereas TG levels were similar (Figure 1C). Of note, the TG/c-HDL ratio is a diagnostic surrogate of NAFLD.<sup>36</sup> A similar but more pronounced phenotype was observed in 6-month-old Lgr4/5dLKO mice. Histologic analysis revealed that livers of ND-fed Lgr4/5dLKO and control mice were similar, but HFD caused livers of Lgr4/5dLKO to develop increased hepatic steatosis compared with control mice (Figure 1, A and B). HFD-fed Lgr4/5dLKO mice displayed reduced levels of serum t-Chol and c-HDL compared with control animals (Figure 1D). TG levels remained unaltered in Lgr4/5dLKO and control mice, irrespective of feeding conditions. Increased serum AST and ALT levels were evident in 6-month-old, but not in 3-month-old, HFD-fed Lgr4/5dLKO mice compared with control mice, respectively, potentially indicating compromised hepatocyte function (Supplemental Figure S1, C and D). More importantly, increased steatosis in 6-month-old HFD-fed Lgr4/5dLKO compared with control mice was not reflected by increased body weight (Supplemental Figure S1E).

Cholesterol and TGs are transported in lipoproteins in the blood. To investigate whether very-low-density lipoprotein (VLDL) secretion was altered, the rate of appearance of TG was measured in serum Lgr4/5dLKO and control mice following poloxamer-407 treatment.<sup>37,38</sup> The amount of VLDL secretion is proportional to the TG increase. Both male and female Lgr4/5dLKO and control mice revealed a similar increase in serum TG levels up to 240 minutes after poloxamer-407 treatment, suggestive of unaltered VLDL

secretion in the Lgr4/5dLKO mice (Figure 1E). To investigate whether lipoprotein composition was altered in our Lgr4/5dLKO mice, FPLC-based size-exclusion chromatography was performed on pooled sera of 3-month-old ND-fed female and male Lgr4/5dLKO and control mice. The fraction comprising VLDL-cholesterol was modestly increased in male and female Lgr4/5dLKO mice, whereas Lgr4/5dLKO mice displayed a remarkable enrichment in serum TG conjugated to VLDL compared with control animals (Figure 1F), analogous to patients with NAFLD.<sup>39</sup> More importantly, the c-HDL fraction was reduced in the Lgr4/5dLKO female and modestly in male mice (Figure 1F). The reduced serum c-HDL content in the Lgr4/5dLKO mice resulted in lower serum t-Chol levels (Figure 1, C, D, and F), because HDL particles are major carriers of cholesterol in mice due to the lack of the cholesteryl ester transfer protein.<sup>40</sup> These results indicate that Lgr4/5dLKO mice exhibit an unaltered VLDL secretion rate, increased serum VLDL-TG, and decreased c-HDL content.

### Lgr4/5dLKO Mice Reveal a NASH-Like Phenotype with Fibrosis

To investigate whether the steatotic phenotype in 6-month-old HFD-fed Lgr4/5dLKO mice was concomitant with additional features of liver disease, the presence of inflammatory cells and mediators was investigated. Steatosis was accompanied by mild hepatic inflammation, as evidenced by slightly elevated levels of ionized calcium-binding adapter molecule 1 (IBA1)-positive macrophages in Lgr4/5dLKO compared with control mice (Supplemental Figure S2, A and B). Furthermore, serum levels of the proinflammatory cytokines, TNF- $\alpha$  and IL-6, were elevated in 6-month-old HFD-fed Lgr4/5dLKO compared with control mice (Supplemental Figure S2, C and D). Livers of 3- and 6-month-old ND- and HFD-fed Lgr4/5dLKO mice were analyzed for fibrotic manifestations. The 6-month-old HFD-fed Lgr4/5dLKO mice showed elevated hepatic collagen networks in their livers compared with 6-month-old HFD-fed control mice, indicative of enhanced hepatic stellate cell activation. No difference was detected in

**Figure 1** Steatosis and serum lipid and lipoprotein imbalance in Lgr4/5dLKO mice. **A:** Hematoxylin and eosin (HE) staining on liver sections of 3- and 6-month-old Lgr4/5dLKO and control mice subjected to normal diet (ND) or 4 weeks of high-fat diet (HFD), respectively. The 6-month-old HFD-fed Lgr4/5dLKO animals developed hepatic steatosis. **Magnified insets** in each panel show representative area; **asterisks** denote steatotic vesicles. **B:** Steatosis quantification based on HE images in **A**. Two-way analysis of variance with 95% CI is shown. **C:** Serum total cholesterol (t-Chol) levels in ND-fed 3-month-old Lgr4/5dLKO mice were lower compared with control mice, whereas cholesterol-high-density lipoprotein (c-HDL) and triglyceride (TG) levels were similar; in 3-month-old HFD-fed Lgr4/5dLKO mice, t-Chol and c-HDL levels were lower compared with control animals, whereas TG levels remained unchanged. Two-way analysis of variance with 95% CI is shown. **D:** Serum t-Chol, c-HDL, and TG levels in ND-fed 6-month-old Lgr4/5dLKO and control mice were similar; in 6-month-old HFD-fed Lgr4/5dLKO mice, t-Chol and c-HDL levels were lower compared with control mice, whereas TG levels were comparable. Two-way analysis of variance with 95% CI is shown. **E:** TG secretion rates were determined in serum of fasted male and female Lgr4/5dLKO and control mice either 5 minutes before (baseline) or 60, 120, and 180 minutes after the onset of poloxamer-407 treatment. TG secretion was similar under all conditions. **F:** Fast protein liquid chromatography (FPLC) analysis on pooled sera of 3-month-old ND-fed mice. HDL-cholesterol was mildly reduced in Lgr4/5dLKO mice, in particular in females [serum HDL-cholesterol (mg/dL): female control and Lgr4/5dLKO mice, 30 and 24, respectively (20% reduction); male control and Lgr4/5dLKO mice, 35 and 30, respectively (14% reduction)]. The **red arrows** denote the content of t-Chol and TG conjugated to very-low-density lipoprotein (VLDL) in female and male mice, respectively. Results are expressed as means  $\pm$  SD (**B–D**).  $n = 5$  ND control, ND Lgr4/5dLKO, HFD control, and HFD Lgr4/5dLKO (**B**);  $n = 18$  ND control (**C**);  $n = 8$  ND Lgr4/5dLKO (**C**);  $n = 6$  HFD control and HFD Lgr4/5dLKO (**C**);  $n = 9$  ND control and HFD Lgr4/5dLKO (**D**);  $n = 11$  ND Lgr4/5dLKO (**D**);  $n = 6$  HFD control (**D**);  $n = 2$  female controls (**F**);  $n = 3$  female Lgr4/5dLKO and male controls (**F**);  $n = 4$  male Lgr4/5dLKO (**F**). \* $P < 0.05$ , \*\* $P < 0.01$ , \*\*\* $P < 0.001$ , and \*\*\*\* $P < 0.0001$ . Scale bar = 100  $\mu$ m (**A**). CV, central vein; HDL, high-density lipoprotein; LDL, low-density lipoprotein; PV, portal vein.



ND-fed 6-month-old mice or in 3-month-old mice when comparing livers of Lgr4/5dLKO with control mice, respectively (Figure 2, A and B). Similarly, increased  $\alpha$ -smooth muscle actin ( $\alpha$ -SMA) levels were present in livers of 6-month-old HFD-fed Lgr4/5dLKO compared with control mice (Figure 2, C and D). To monitor the predisposition of Lgr4/5dLKO mice to liver fibrosis using a noninvasive diagnostic device, 3- and 6-month-old ND-fed Lgr4/5dLKO and control mice were subjected to liver ultrasound elastography. Although liver stiffness in 3-month-old mice was comparable (data not shown), 6-month-old ND-fed Lgr4/5dLKO female mice tended to have stiffer livers compared with control animals (Supplemental Figure S2E). These findings are in line with increased fibrotic manifestations observed in 6-month-old HFD-fed Lgr4/5dLKO mice (Figure 2). In summary, these data strongly support the notion that mice with decreased Wnt/ $\beta$ -catenin signaling on Lgr4/5 deletion were prone to develop a NASH-like phenotype accompanied by fibrosis.

### Changes in Lipid and BA Metabolism and Extracellular Matrix Remodeling in Lgr4/5dLKO Hepatocytes

Lipid accumulation can result from dysregulated free FA uptake from blood, enhanced *de novo* lipogenesis, increased chylomicron remnant hepatic uptake, or diminished secretion.<sup>41</sup> To address the mechanism of steatosis in our Lgr4/5dLKO mice, bulk RNA-sequencing analysis was performed on livers derived from 1-month-old ND-fed Lgr4/5dLKO and control mice to capture causative transcriptome changes that preceded the phenotypic manifestation observed in 3- and 6-month-old ND- and HFD-fed mice. Livers of 1-month-old Lgr4/5dLKO mice did not display any visible lipid accumulation (Supplemental Figure S3A). Yet, the transcriptome analysis revealed several genes that were strongly down-regulated or mildly up-regulated (Figure 3A). Among the former, the study identified several genes encoding transporter proteins, indicative of altered intercellular transport function in livers of Lgr4/5dLKO mice. Pathway enrichment analysis was performed on the down-regulated and up-regulated genes to gain mechanistic insights into the biological consequences of *Lgr4/5* gene disruption. The main down-regulated pathways comprised metabolism and synthesis of lipids, steroids, BAs, and bile salts as well as transport of bile salts, organic

acids, small molecules, and solute carrier-mediated transmembrane transport (Figure 3B). Up-regulated pathways consisted of extracellular matrix organization and degradation, integrin and nonintegrin interactions, collagen cross-linking, trimerization and degradation, glycosylation, and neural cell adhesion molecule and platelet-derived growth factor signaling (Figure 3C). Gene regulatory network analysis was conducted on the down-regulated genes to elucidate coregulatory events by master transcription factors responsible for decreased gene expression in livers of Lgr4/5dLKO compared with control mice (Figure 3D). On the basis of transcription factor motif enrichment analysis, transcription factor 7-like 2 (*Tcf7l2*) and nuclear receptor subfamily 1 group D member 2 (*Nr1d2*; *Rev-Erb $\beta$* ) emerged as the two master regulators for down-regulated genes. The Wnt pathway effector TCF7L2 interacts with  $\beta$ -catenin and regulates hepatic metabolic gene expression, and NR1D2 is a nuclear receptor that acts as a transcriptional repressor, regulating processes in the development of NAFLD.<sup>42,43</sup> The current data suggested that loss of Wnt/ $\beta$ -catenin signaling in hepatic epithelial cells of 1-month-old Lgr4/5dLKO mice led to TCF7L2- and NR1D2-mediated transcription repression of metabolic and lipid homeostasis genes, thereby predisposing the liver to develop a fatty liver phenotype. In summary, these transcriptome data suggest a deficit in lipid and BA metabolism and an increased extracellular matrix remodeling propensity in hepatocytes derived from 1-month-old Lgr4/5dLKO compared with control mice, predisposing to compromised cellular function in mice at higher age.

### Liver Steatosis Correlates with Loss of BA Secretion from Lgr4/5dLKO Hepatocytes

To investigate how the reduced serum lipid levels in Lgr4/5dLKO mice (Figure 1C) correlated with hepatic lipid content, freshly isolated primary hepatocytes from 3-month-old ND-fed Lgr4/5dLKO and control mice were starved overnight in basal serum-free medium. The lipid content was then evaluated using a hydrophobic BODIPY FL dye.<sup>44</sup> The *ex vivo* cultures revealed that the Lgr4/5dLKO hepatocytes contained lipids stored in enlarged droplets compared with control hepatocytes (Figure 4A). To assess whether lipid accumulation in Lgr4/5dLKO hepatocytes was caused by altered clearance of low-density

**Figure 2** Liver fibrosis in 6-month-old high-fat diet (HFD)-fed Lgr4/5dLKO mice. **A:** Picrosirius red staining in liver sections of 3- and 6-month-old normal diet (ND)- and HFD-fed mice. **Arrows** denote collagen fibers. **B:** Collagen quantification based on picrosirius red staining in **A**. The 6-month-old HFD-fed Lgr4/5dLKO mice contained increased levels of collagen compared with 6-month-old HFD-fed control mice, indicating a higher degree of fibrosis. The 3- and 6-month-old ND-fed Lgr4/5dLKO mice and 3-month-old HFD-fed Lgr4/5dLKO mice also trended toward increased collagen content compared with the respective control animals, but the differences did not reach statistical significance. Two-way analysis of variance with 95% CI is shown. **C:**  $\alpha$ -Smooth muscle actin ( $\alpha$ -SMA) and hematoxylin staining on liver sections of 3- and 6-month-old ND- and HFD-fed female mice. **Arrows** denote  $\alpha$ -SMA-positive areas. **D:**  $\alpha$ -SMA quantification based on  $\alpha$ -SMA and hematoxylin staining in **C**. The 6-month-old HFD-fed Lgr4/5dLKO mice contained increased  $\alpha$ -SMA staining compared with 6-month-old HFD-fed control mice, revealing increased hepatic stellate cell activation. The 3- and 6-month-old ND-fed Lgr4/5dLKO mice and 3-month-old HFD-fed Lgr4/5dLKO mice also trended toward increased  $\alpha$ -SMA staining compared with the respective control animals, but the differences did not reach statistical significance. Two-way analysis of variance with 95% CI is shown. Results are expressed as means  $\pm$  SD (**B** and **D**).  $n = 5$  ND control, ND Lgr4/5dLKO, HFD control, and HFD Lgr4/5dLKO (**B** and **D**).  $*P < 0.05$ . Scale bars = 50  $\mu$ m (**A** and **C**). CV, central vein; PV, portal vein.

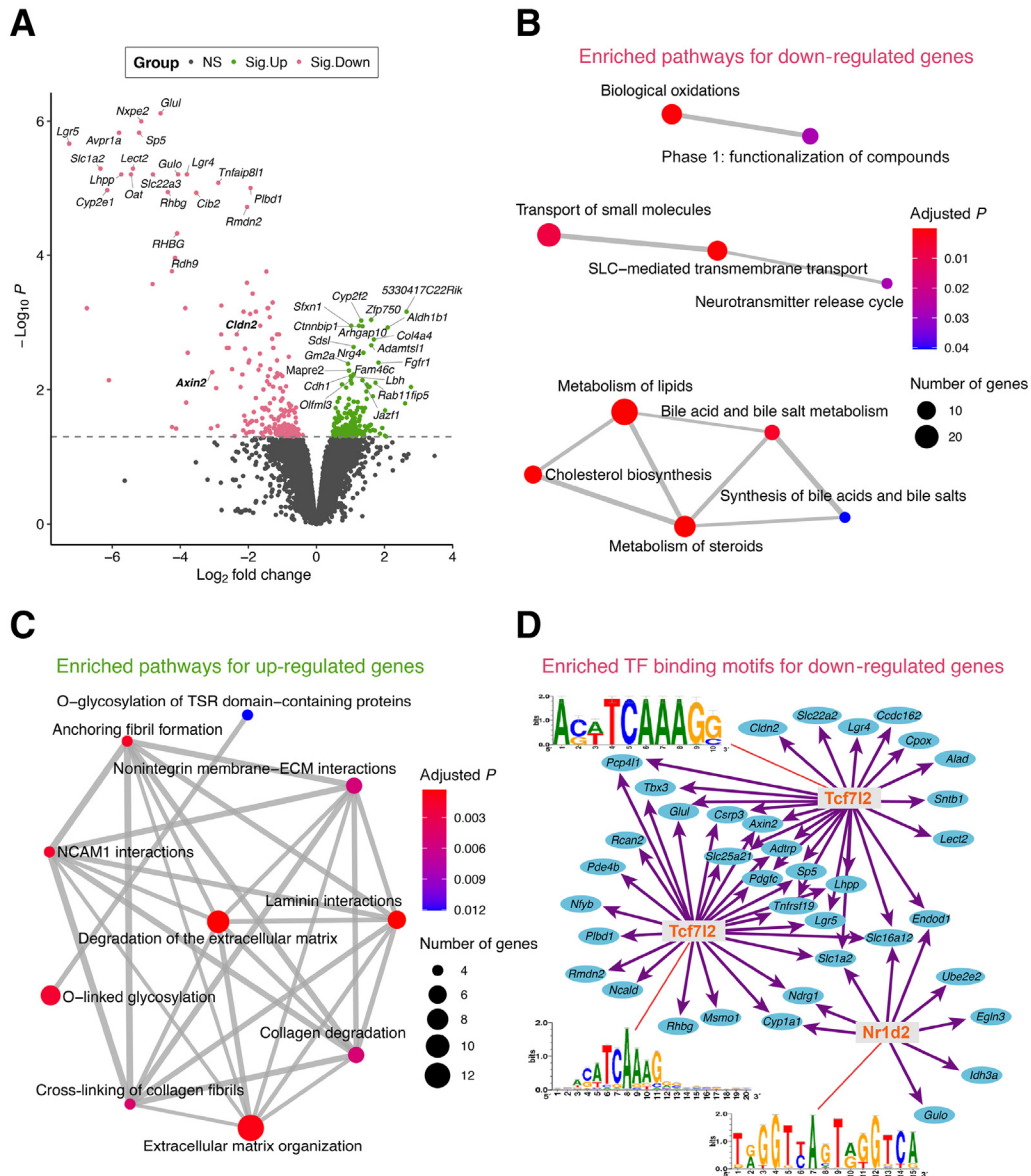


**Figure 3** Livers of 1-month-old normal diet-fed *Lgr4/5dLKO* mice indicate differential regulation of a subset of genes. **A:** Volcano plot of differential gene expression analysis between *Lgr4/5dLKO* and control mice. The dashed gray line indicates the cutoff for statistical significance; adjusted  $P < 0.05$ . Only the top 20 up-regulated or down-regulated genes are labeled with gene symbols. Significantly up-regulated (Sig.Up) and down-regulated (Sig.Down) genes in *Lgr4/5dLKO* mice are shown in green and pink, respectively. *Cldn2* and *Axin2* were additionally marked for discussion in Results. **B** and **C:** Pathway enrichment analysis for the 217 down-regulated (**B**) and 203 up-regulated (**C**) genes. Dot size represents the number of genes involved in each pathway. Dot color indicates the statistical significance (adjusted  $P$  value) for each pathway. The thickness of the line connecting two pathways reflects the number of shared genes between the pathways. The more the shared genes, the thicker the line. **D:** Gene regulatory networks of the top three motifs [corresponding to two master regulators, nuclear receptor subfamily 1 group D member 2 (NR1D2) and transcription factor 7 like 2 (TCF7L2)] and their target genes among the down-regulated genes in *Lgr4/5dLKO* mice. ECM, extracellular matrix; NCAM, neural cell adhesion molecule; NS, not significant; SLC, solute carrier; TSR, thrombospondin type 1 repeat.

lipoprotein (LDL) from plasma, the competence of *Lgr4/5dLKO* hepatocytes to take up LDL vesicles *ex vivo* was tested. Freshly isolated hepatocytes from livers of both 6-week-old control and *Lgr4/5dLKO* mice were maintained as two-dimensional monolayer cultures, as depicted in Supplemental Figure S3B. On day 2, hepatocytes were incubated with LDL vesicles conjugated to the red fluorophore Phrodo (LDL-Phrodo), and the kinetics of uptake was determined by measurements after 5, 10, 15, 20, and 24 hours of LDL-Phrodo addition. To distinguish between

newly incorporated LDL vesicles and lipids existing in lipid droplets, LDL-Phrodo was removed after 24 hours (day 3), and cells were incubated for 1 minute with BODIPY FL. *Lgr4/5dLKO* hepatocytes revealed a reduced LDL vesicle uptake compared with control cells (Figure 4B) but contained abundant levels of endogenous lipid droplets (Figure 4C). These results demonstrate that enhanced lipid accumulation in *Lgr4/5dLKO* hepatocytes was not a consequence of enhanced LDL uptake. In line with the findings on compromised lipid and BA metabolism in

Lgr4/5dLKO mice, decreased expression of *Cldn2* suggested that the BA-mediated export mechanism was altered (Figure 3A). To assess the BA secretory ability of Lgr4/5dLKO hepatocytes, primary hepatocytes were isolated from livers of 6-week-old ND-fed Lgr4/5dLKO and control mice and cultivated in a three-dimensional collagen-Matrigel sandwich format over 7 days, the period necessary to recreate functional canaliculi *ex vivo*.<sup>45</sup> The fluorescent BA analog CLF<sup>46</sup> was utilized to quantify the BA efflux from hepatocytes, according to the scheme depicted in Supplemental Figure S3C. Initiation of canalicular network formation in control and Lgr4/5dLKO hepatocytes started 2 days after seeding, whereby control cells showed an increased speed of canalicular structure development. On day 3, both control and Lgr4/5dLKO hepatocyte cultures displayed similarly organized canalicular networks (Figure 4D). On day 7, Lgr4/5dLKO hepatocytes had strikingly reduced CLF secretion into bile canaliculi compared with control cells (Figure 4D). In humans, defects in canalicular secretion with progressive intrahepatic trapping of BAs induce hepatocellular injury, biliary fibrosis, and end-stage liver disease.<sup>47</sup> To determine whether the compromised BA flow was due to altered hepatic junctions in Lgr4/5dLKO mice, the study evaluated the integrity of adherens junctions by studying the hepatic localization of cadherin 1 (CDH1),<sup>48</sup> whose expression was increased in livers of 3-month-old ND-fed Lgr4/5dLKO mice (Figure 4E). CDH1 is known to interact with the Wnt pathway effector protein  $\beta$ -catenin (CTNNB1), whose expression (*Ctnnb1*) was unaltered, whereas the Wnt/ $\beta$ -catenin target gene axis inhibition protein 2 (*Axin2*) was strongly reduced (Figure 4E). CDH1 and CTNNB1 revealed a similar colocalization in livers of 3-month-old ND-fed Lgr4/5dLKO and control animals, respectively, suggesting that the interaction of these proteins was unaltered in adherens junctions (Figure 4F). Furthermore, TJs of 3-month-old ND-fed Lgr4/5dLKO mice appeared morphologically intact, as analyzed by transmission electron microscopy and immunofluorescence analysis of the tight junction protein zona occludens protein-1 (Figure 4G). Similarly, livers of *Cldn2*<sup>-/-</sup> mice revealed a normal bile canaliculi structure.<sup>8</sup> These data imply that bile canaliculi functionality is not affected by abnormal TJ formation. These results suggest that loss of BA secretion in Wnt/ $\beta$ -catenin-impaired mouse livers was caused by changes in cellular physiology and extracellular matrix remodeling, rather than by abnormal hepatic junctions.

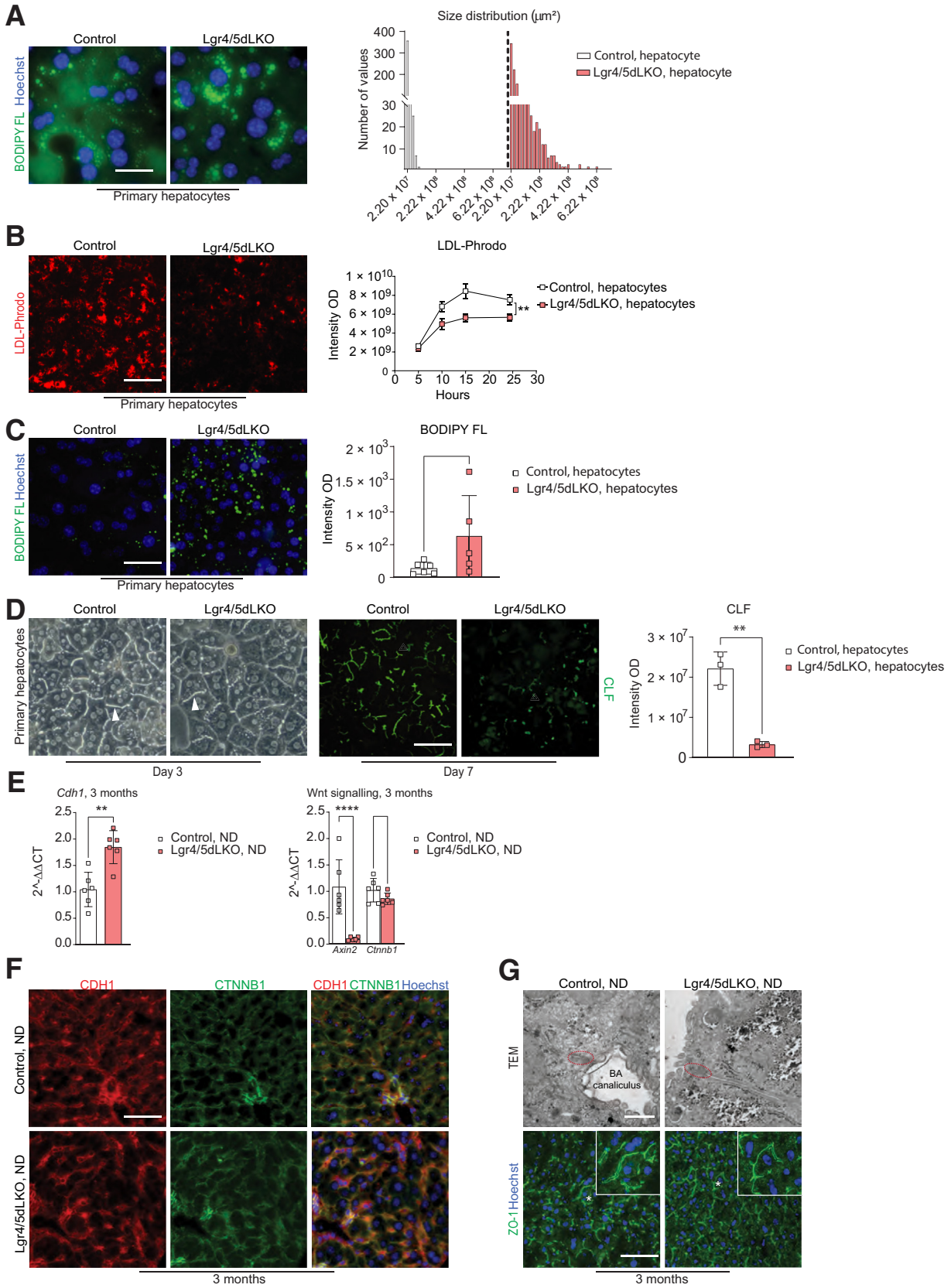
### Cholestatic Phenotype of ND-Fed Lgr4/5dLKO Mice

Loss of hepatic BA secretion is expected to result in altered BA homeostasis. Hence, levels of individual conjugated and unconjugated BAs were determined in liver, bile, plasma, and feces of Lgr4/5dLKO and control mice. In addition, levels of C4, a marker of hepatic Cyp7a1 activity and bile acid biosynthesis,<sup>49</sup> were also measured in liver

and plasma. Lgr4/5dLKO mice exhibited strong statistically significant increases in total BAs (sum of individual BA components measured) (Supplemental Figure S4, A–C, and Supplemental Table S1) in liver and plasma, associated with decreased total BAs in feces (Figure 5, A–C). Although overall total BA concentrations were unchanged in bile of Lgr4/5dLKO compared with control mice, some of the major individual BA components in bile fluid were statistically significantly decreased, such as taurodeoxycholic acid (TDCA), taurochenodeoxycholic acid (TCDCA), tauroursodeoxycholic acid (TUDCA), and tauro- $\alpha$ -muricholic acid (TaMCA) (Figure 5D, Supplemental Figure S4D, and Supplemental Table S1). Concentrations of liver and plasma C4 were strongly decreased in Lgr4/5dLKO animals (Figure 5, E and F), suggesting a feedback loop activation in response to accumulating BAs in hepatocytes as a compensatory mechanism to decrease BA production under cholestatic conditions. There was no obvious shift toward a subset of bile acid components or any of the two major biosynthetic pathways (ie, cholic acid or chenodeoxycholic synthesis pathway) in Lgr4/5dLKO mice.

To examine whether the altered BA homeostasis occurred due to changes in cellular transporters in the liver, the expression of BA and cholesterol transporters was analyzed in 1- and 3-month-old<sup>20</sup> Lgr4/5dLKO and control mice. Only a few transporters were decreased in livers of Lgr4/5dLKO mice compared with control mice, including the solute carrier organic anion transporter family member 1b2 (*Slco1b2*) in 1- and 3-month-old mice and *Slco1a5* in 1-month-old mice (Supplemental Figure S5A). The BA transporter *SLCO1B2* is expressed in the basolateral plasma membrane of hepatocytes and involved in the hepatic uptake of unconjugated bile acids.<sup>50</sup> That *SLCO1B2* also mediates efflux of BAs from hepatocytes under conditions of high BA concentrations in hepatocytes cannot be excluded.<sup>51</sup> Given that only few BA transporters manifested changes in gene expression in Lgr4/5dLKO mice, it is unlikely that solely altered transporter expression was causal for the severe cholestatic phenotype observed in these mice. Therefore, cytochrome (*Cyp*) gene expression in the same mice was analyzed to investigate whether altered *Cyp* expression could be responsible for the disturbed BA homeostasis. A few *Cyp* genes showed decreased expression in Lgr4/5dLKO mice (eg, *Cyp1a1* and *Cyp1a2* in livers of 1-month-old mice, *Cyp27a1* in 3-month-old mice, and *Cyp51* in both age groups) (Supplemental Figure S5B). CYP1A1 and CYP51 have been linked to cholesterol metabolism, whereas CYP27A1 is an essential enzyme in BA biosynthesis, catalyzing the oxidation step of the cholesterol side chain to form BAs. CYP1A1 has a protective role against NAFLD in mice.<sup>52,53</sup> It is therefore conceivable that these CYP proteins contributed to the cholestatic phenotype in the Lgr4/5dLKO mice.

Taken together, Lgr4/5dLKO mice showed features of cholestasis, as characterized by increased BAs in plasma



and BA accumulation in the liver. This was consistent with decreased canalicular efflux/secretion, as indicated by the clear decrease in total feces BA content and the decrease in some individual BA components in bile fluid.

### Livers of Lgr4/5dLKO Mice Reveal Altered Lipid Profiles

Triggered by the steatotic liver phenotype in Lgr4/5dLKO mice, lipid analysis was performed on livers of 6-month-old Lgr4/5dLKO and control mice that were fed with either ND or HFD. HFD-fed Lgr4/5dLKO mice displayed an increase in several lipid species compared with ND, in particular TG. HFD-fed Lgr4/5dLKO mice had higher levels of 45 different species of TGs,<sup>54</sup> 16 diacylglycerols, 10 oxidized TGs, 8 TG-estolides,<sup>55</sup> and 4 phosphatidylglycerols compared with ND-fed Lgr4/5dLKO mice (Figure 6A). In contrast, fewer lipids were up-regulated in control mice comparing HFD with ND conditions (ie, 16 different species of TG, 8 diacylglycerols, 3 phosphatidylglycerols, and 2 FA esters of hydroxy FA).<sup>56</sup> Regarding the fatty acyl composition of significantly up-regulated TGs, livers of HFD-fed Lgr4/5dLKO mice contained a more diverse FA pool, including several polyunsaturated forms, in particular 16:3, 18:3, 20:5, 21:3, 22:3, 22:5, and 22:6 (Figure 6B), compared with those of HFD-fed control mice. The complete list of increased and decreased lipid species on HFD compared with ND, in both control and Lgr4/5dLKO mice, is shown in Supplemental Table S2. The data show that Lgr4/5dLKO mice exhibited a different lipid response to the HFD challenge compared with control mice, in particular an increase in several species of unsaturated TGs, revealing altered lipid homeostasis.

### Wnt Pathway Modulation in Humans with Liver Cirrhosis

To explore whether fatty liver disease in humans is associated with decreased levels of *LGR4* and *LGR5* expression, mRNA *in situ* hybridization on human healthy, NASH, and cirrhotic liver specimens was performed. *LGR4* mRNA was expressed

in hepatocytes and cholangiocytes of normal, NASH, and cirrhotic livers, whereas *LGR5* mRNA expression was restricted to pericentral hepatocytes of normal and NASH specimens (Supplemental Table S3), suggestive of loss of *LGR5* expression in cirrhotic livers. To investigate whether decreased Wnt pathway activity is associated with cirrhosis in humans, a consequence of NAFLD, the expression of Wnt target genes was analyzed in human hepatocytes using published single-cell RNA-sequencing data derived from normal and cirrhotic human livers.<sup>57,58</sup> *Cyp1a2* and *Cyp2e1*<sup>59</sup> and *Glul*<sup>20</sup> are Wnt target genes expressed in mouse liver, and were strongly decreased in livers of 1-month-old ND-fed Lgr4/5dLKO compared with control mice (Supplemental Figure S6A). Analyzing the human orthologs of these genes *CYP1A2*, *CYP2E1*, and *GLUL* in the human single-cell RNA data set revealed that their expression was also significantly decreased in hepatocytes from human cirrhotic livers, suggesting decreased Wnt pathway activity (Supplemental Figure S6B).

### Discussion

Increasing evidence suggests that Wnt/ $\beta$ -catenin signaling plays a role in both exogenous and endogenous lipid trafficking and biliary homeostasis, but the physiological consequences of Wnt/ $\beta$ -catenin pathway activity on hepatic metabolic functions and NAFLD development are incompletely understood. To address this question, the current study investigated phenotypic manifestations in liver and serum of mice devoid of Lgr4/5 in hepatic epithelial cells, two components that are crucial for regulating liver Wnt/ $\beta$ -catenin pathway activity.<sup>20,60</sup> The data show that abrogation of Wnt/ $\beta$ -catenin activity led to fat accumulation in the liver, partly due to defective BA secretion, concomitant with increased liver inflammation and a predisposition to fibrosis.

The increased steatosis and resistance to diet-induced obesity observed in the Lgr4/5dLKO mice fed with HFD is in line with findings from  $\beta$ -catenin KO mice.<sup>22</sup> Similarly, LDL receptor-related protein 6 (*Lrp6*) mutant mice showed

**Figure 4** Hepatic lipid accumulation associated with decreased BA secretion in Lgr4/5dLKO hepatocytes. **A:** BODIPY FL staining of primary hepatocytes isolated from 3-month-old normal diet (ND)-fed mice. Frequency distribution of lipid droplet size (area expressed in  $\mu\text{m}^2$ ) was measured 24 hours after seeding. Lipid droplets in Lgr4/5dLKO hepatocytes differed in number and size from control cells (number of lipid droplets analyzed in control, >400, and in Lgr4/5dLKO, >1500). The **black dashed line** represents the visual separation of data derived from hepatocytes of control mice (**left side**) and Lgr4/5dLKO mice (**right side**). **B:** Hepatocytes from 6-week-old Lgr4/5dLKO mice revealed significantly reduced low-density lipoprotein (LDL) vesicle uptake compared with control cells (two-way analysis of variance with Sidak test was used). LDL-Phrodo (red dots) images refer to the 24-hour time point. **C:** BODIPY FL staining on hepatocytes at 24 hours in culture after onset of LDL-Phrodo addition. Note the abundant content of endogenous lipid droplets in hepatocytes from Lgr4/5dLKO mice (*t*-test,  $P = 0.08$ , statistical significance not reached). **D:** Bright-field and fluorescent images of collagen-Matrigel three-dimensional hepatocyte cultures 3 days and 7 days after cell seeding, respectively. The canaliculi network in Lgr4/5dLKO and control hepatocytes is exemplified by **arrowheads**. Cholyl-L-lysyl-fluorescein (CLF) assays demonstrated a loss of BA secretion from Lgr4/5dLKO hepatocytes on day 7 (*t*-test was used). **E:** *Cdh1* gene expression in livers of 3-month-old Lgr4/5dLKO mice was increased (*t*-test was used). Although *Axin2* gene expression was abolished in 3-month-old ND-fed Lgr4/5dLKO mice, *Ctnnb1* gene expression was comparable to control animals (*t*-test was used). **F:** Cadherin 1 (CDH1) and  $\beta$ -catenin (CTNNB1) immunofluorescence staining on paraffin-embedded liver sections of 3-month-old ND-fed Lgr4/5dLKO and control animals showed that the colocalization of CDH1 and CTNNB1 was intact in the Lgr4/5dLKO mice. **G:** Transmission electron microscopy (TEM) and zona occludens protein-1 (ZO-1) staining confirmed the presence of intact tight junctions in 3-month-old ND-fed Lgr4/5dLKO mice (circled areas in the TEM panels). The **magnified insets** in the ZO-1 Hoechst panels (control, ND; Lgr4/5dLKO, ND) represent twofold magnifications of areas containing a cell, each, as marked by **white asterisks**. Results are expressed as means  $\pm$  SD (**B–E**).  $n = 2$  biological replicates (**B** and **C**);  $n = 6$  technical replicates (**B** and **C**);  $n = 5$  Lgr4/5dLKO (**C**);  $n = 3$  technical replicates (**D**);  $n = 6$  control animals and Lgr4/5dLKO (**E**).  $^{**}P < 0.01$  and  $^{****}P < 0.0001$ . Scale bars: 20  $\mu\text{m}$  (**A**); 50  $\mu\text{m}$  (**B–D** and **F**); 500 nm (**G**, TEM); 100  $\mu\text{m}$  (**G**, ZO-1 Hoechst).

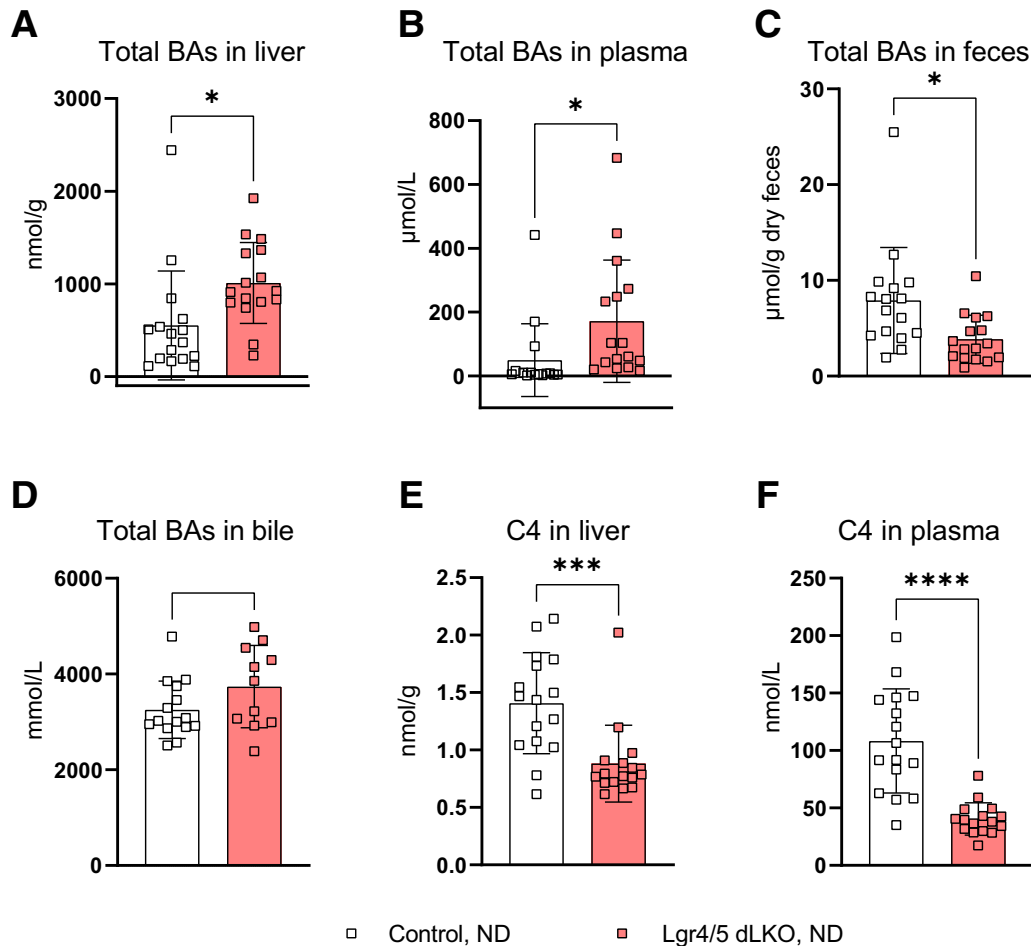


**Figure 5** Disturbed BA homeostasis in *Lgr4/5*dLKO mice. **A–C:** Total BAs were increased in liver (**A**) and plasma (**B**), but decreased in feces (**C**), of normal diet (ND)–fed *Lgr4/5*dLKO mice compared with control mice. **D:** Total BAs in bile were similar in both *Lgr4/5*dLKO and control mice, whereas some individual bile acid species were decreased in *Lgr4/5*dLKO mice (Supplemental Figure S4D). **E and F:** The 7 $\alpha$ -hydroxy-4-cholesten-3-one (C4) in liver (**E**) and plasma (**F**) was decreased in *Lgr4/5*dLKO mice compared with control mice. The following animals were investigated: 8 female *Lgr4/5*dLKO mice, 13 to 14 weeks old; 8 female control mice, 10 to 14 weeks old; 8 male *Lgr4/5*dLKO mice, 12 to 15 weeks old; and 8 male control mice, 12 to 15 weeks old. Respective samples from all animals were used for the study, except for bile probes from male mice, where samples could only be harvested from 7 control and 3 *Lgr4/5*dLKO mice. Statistical significance determined by two-tailed, unpaired *t*-test: \**P* < 0.05, \*\*\**P* < 0.001, and \*\*\*\**P* < 0.0001. BA, bile acid.

enhanced hepatic *de novo* lipogenesis and lipid and cholesterol biosynthesis, resulting in elevated hepatic fat, TG, and cholesterol ester content, progressing toward NAFLD.<sup>25</sup> Loss-of-function point mutations in the *LRP6* gene lead to early onset of serum hyperlipidemia and metabolic syndrome in humans and engineered mice.<sup>25,61</sup> Hepatocyte-specific  $\beta$ -catenin knockout mice developed hepatic steatosis when fed with methionine- and choline-deficient diet but not with HFD. Collectively, this suggests that abrogated Wnt/ $\beta$ -catenin promotes NAFLD and NASH.

In contrast, Wnt/ $\beta$ -catenin activation on hepatic epithelial cell-specific ectopic  $\beta$ -catenin expression in mice fed with HFD<sup>22</sup> or through loss of the ZNRF3/RNF43 module, mediated by AAV8-TBG-Cre or Alb-Cre-ERT2 (designated *Rnf43/Znrf3*<sup>del</sup>),<sup>21</sup> was described to cause hepatic steatosis. These studies provided insights about the role of the  $\beta$ -catenin transcriptional regulator in the context of liver metabolic disorders. It remains unclear why *Rnf43/*

*Znrf3*<sup>del21</sup> caused NAFLD and NASH, whereas our mice with Ad5-Cre–mediated deletion of *Znrf3/Rnf43* (referred to as Ad5-Cre-*Znrf3/Rnf43*<sup>KO</sup>)<sup>23</sup> showed the opposite phenotype. Although control mice developed significant age-related steatosis, our aged Ad5-Cre-*Znrf3/Rnf43*<sup>KO</sup> mice were protected from hepatic fat accumulation.<sup>23</sup> Moderate steatosis was observed in a subset of liver tumors that developed in our Ad5-Cre-*Znrf3/Rnf43*<sup>KO</sup> mice, but the degree of steatosis was less than that in the livers of age-matched control littermates.<sup>23</sup> Interestingly, livers of both *Rnf43/Znrf3*<sup>del</sup> mutant mice<sup>21</sup> and the *Lgr4/5*dLKO mice described in this study revealed altered lipid homeostasis. However, the *Rnf43/Znrf3*<sup>del</sup> mutant mice showed increased phospholipids and diacylglycerols containing four or five double bonds,<sup>21</sup> whereas our HFD-fed *Lgr4/5*dLKO mice revealed increased TG, including polyunsaturated species with up to six double bonds, oxidized TGs, TG-estolides, and diacylglycerols. Recent evidence has described LGR4

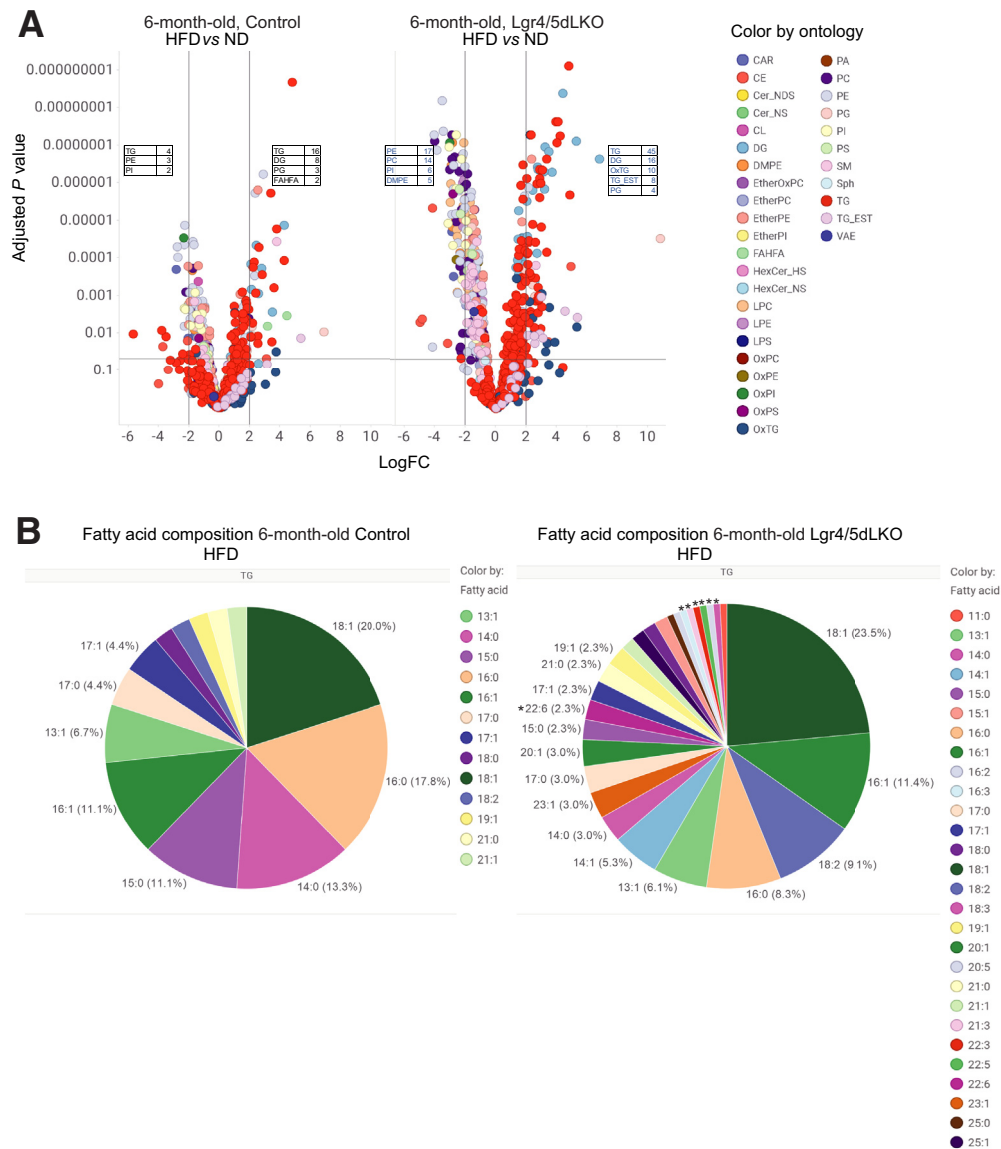


**Figure 6** Lipid changes in livers of Lgr4/5dLKO mice. **A:** Volcano plots depicting lipid species found increased and decreased in livers of 6-month-old high-fat diet (HFD)– versus normal diet (ND)–fed Lgr4/5dLKO and control mice, respectively. HFD-fed Lgr4/5dLKO mice showed a significantly higher number of triglycerides (TGs), diacylglycerols (DGs), oxidized TGs (OxTGs), TG-estolides (TG-ESTs), and phosphatidylglycerols (PGs) compared with ND-fed Lgr4/5dLKO mice. Lipid changes with adjusted  $P > 0.05$  and  $\log_2$  fold change  $> 2$  were considered as significantly changed. Tables depicted in volcano plots (black fonts for control, and blue fonts for Lgr4/5dLKO) display the number of different lipid species identified, grouped by ontology, as either increased or decreased on HFD compared with ND (right and left, respectively, in each graph). Abbreviations were used according to Nomenclature in MS-DIAL Lipidomics (<http://prime.psc.riken.jp/compms/msdial/lipidnomenclature.html>, last accessed April 21, 2021). **B:** Pie chart representation of the distribution of specific TG fatty acyl species in HFD-fed Lgr4/5dLKO and control mice (expressed in percentage). Note that several fatty acyl species were only detected in livers of Lgr4/5dLKO mice, a fraction as polyunsaturated fatty acyl form. The asterisk indicates TG fatty acyl species with three or more double bonds. FAHFA, FA esters of hydroxy FA.

as a key regulator in lipid metabolism, in both adipose tissue and liver.<sup>62,63</sup> Therefore, it is conceivable that the incapability of Lgr4/5dLKO hepatocytes to secrete BAs, in addition to defective hepatic FA oxidation by abrogated Wnt/ $\beta$ -catenin signaling,<sup>22</sup> led to increased FA unsaturation and subsequent storage in large lipid droplets. Interestingly, increased levels of TG-estolides were identified in the livers of 6-month-old HFD-fed Lgr4/5dLKO mice. TG-estolides are TG-bound FA esters of hydroxy FA and represent a

major storage form of bioactive free FA esters of hydroxy FA.<sup>55</sup> FA esters of hydroxy FA represent a large family of lipids with poorly understood biological functions, including immunomodulatory activities.<sup>56</sup> It is plausible that the presence of these lipids reflected the need of the hepatocytes to cope with increased hepatic lipid load and/or to induce liver inflammation, causing the onset of NASH. Although the current data support the notion that abrogated Wnt/ $\beta$ -catenin signaling promoted NALFD, more research

is required by studying the detailed differences between the *Rnf43/Znrf3<sup>del</sup>* and *Ad5-Cre-Znrf3/Rnf43<sup>KO</sup>* models to explain this discrepancy. Yet, Wnt pathway effectors, such as LRP5/6 receptors and  $\beta$ -catenin, are involved in several physiological functions distinct from canonical Wnt/ $\beta$ -catenin transcriptional activation. For instance, LRP5/6 contain three copies of the LDL type-A motif, known to mediate the binding and the endocytosis of lipoproteins.<sup>25</sup> Similarly,  $\beta$ -catenin is a protein involved in the regulation and coordination of cell-cell junctions, a structural cellular component whose integrity is coupled with TJ formation (reviewed by Campbell et al<sup>64</sup>). Therefore, it is plausible that the impact of LRP5/6 and  $\beta$ -catenin on NAFLD etiology results from a combination of impacted Wnt signaling, altered lipoprotein uptake, and cell-cell contact.

NAFLD etiology can be the result of a combination of abnormalities in fat and amino acid metabolism, orchestrated by pericentral and periportal hepatocytes. Although the role of Wnt/ $\beta$ -catenin signaling in metabolic liver zonation is well characterized, the consequences of impaired metabolic processes and how they may promote NAFLD are less clear. In patients with NAFLD, lipid accumulation normally initiates in lipid droplets within pericentral hepatocytes.<sup>65,66</sup> This lipid zonation is gradually lost during disease progression.<sup>67</sup> Recent evidence points toward a role of LGR4 in energy metabolism and metabolic diseases (reviewed by Yang et al<sup>68</sup>). Mutations in the *LGR4* gene in humans have been linked to type 2 diabetes with hypertension and central obesity.<sup>69,70</sup> Furthermore, genome-wide association studies have identified an association of the *RSPO3* locus with type 2 diabetes and insulin resistance,<sup>71</sup> and a meta-analysis of multiple genome-wide association studies has identified the *RSPO3* locus to be associated with the waist/hip ratio, which is a measure of body fat distribution and a predictor of metabolic diseases.<sup>72</sup> Given the high prevalence of NAFLD in type 2 diabetes,<sup>73</sup> it is conceivable that mutations in the *RSPO-LGR4/5* node lead to the predisposition of NAFLD development in humans. A transcriptome profiling study in human liver tissue, representing NAFLD progression, showed that genes involved in Wnt signaling were decreased in NASH specimens compared with normal tissue.<sup>74</sup> Furthermore, polyunsaturated FAs were elevated in livers of HFD-fed *Lgr4/5dLKO* compared with HFD-fed control mice, and polyunsaturated FAs were positively related to the risk of NAFLD in a human population.<sup>75</sup>

Wnt/ $\beta$ -catenin signaling regulates BA biosynthesis in perivenous hepatocytes.<sup>6,7</sup> Liver-specific deletion of the canonical Wnt pathway effector protein  $\beta$ -catenin leads to accumulation of hepatic cholesterol and BAs, elevation of serum bilirubin, increased steatohepatitis, and fibrosis in mice fed with a steatogenic methionine- and choline-deficient diet,<sup>24</sup> suggesting a putative defect in BA secretion due to dilated and tortuous bile canaliculi.<sup>76</sup> Inactivation of Wnt/ $\beta$ -catenin signaling causes strongly reduced expression of the perivenous membrane protein CLDN2,

which participates in the formation of intercellular TJs. CLDN2 is involved in BA and water flow regulation in bile canaliculi, and deletion of *Cldn2* in polarized hepatocyte-like cells caused a disruption of functional bile canaliculus-like structures.<sup>8,9</sup> The importance of  $\beta$ -catenin for bile canaliculi formation was demonstrated in hepatocytes derived from a dual  $\beta$ -catenin and  $\gamma$ -catenin mouse KO model.<sup>77</sup> In contrast, the current study found intact TJs in livers of our *Lgr4/5dLKO* mice, and hepatocytes isolated thereof, revealed normal canalicular network formation. *Ctnnb1* expression in the *Lgr4/5dLKO* mice was not altered, thus explaining the different phenotype. Our *ex vivo* hepatocyte and transcriptomic data extended these findings and implied that BA production and secretion were compromised in the *Lgr4/5dLKO* mice. *Lgr4/5* deletion promoted loss of *Cldn2* gene expression, which was accompanied by reduced BA secretion from hepatocytes, suggesting a potential impairment of the endogenous lipid export pathway. Indeed, the reduction of transmembrane transporters and the alterations in BA metabolism identified in our transcriptome analysis in livers of the *Lgr4/5dLKO* mice highly correlated with functional impairment of BA homeostasis. The increase in total BAs in liver and plasma and the decrease in total BAs in feces and in a subset of BAs in the bile of *Lgr4/5dLKO* mice reflected the distorted BA secretion *in vivo*, expanding on the findings in the *ex vivo* *Lgr4/5dLKO* hepatocyte cultures. Despite signs of activation of a potential compensatory feedback loop, negative consequences caused by loss of LGR4/5 on BA secretion appeared to outweigh this likely compensatory mechanism, leading to a cholestatic phenotype. These cholestatic features likely intersect with features of NAFLD, because cholestasis and NAFLD share certain pathophysiological mechanisms that could be targeted by therapeutic intervention.<sup>78</sup>

The endogenous lipid trafficking route comprises the import and export of lipids into and from the liver by LDL and VLDL particles, respectively. Inadequate export of VLDL represents a central, incompletely understood mechanism in patients developing NAFLD. Although individuals with simple steatosis exhibit increased VLDL-TG secretion, patients harboring genetic mutations that cause abnormal VLDL assembly or reduced VLDL export manifest an augmented risk to develop NASH.<sup>79,80</sup> Wnt/ $\beta$ -catenin signaling impinges on VLDL and the VLDL receptor. Knockdown of the VLDL receptor in retinal pigment epithelium results in the elevation of LRP6 protein levels and activation of Wnt/ $\beta$ -catenin signaling, whereas overexpression of the VLDL receptor suppresses Wnt signaling.<sup>81</sup> Our *Lgr4/5dLKO* mice unveiled subphysiological serum t-Chol and c-HDL but modestly increased serum VLDL-cholesterol and strongly elevated VLDL-TG levels, likely due to a compensatory response toward intracellular hepatic lipid accumulation. These findings are supported by the disturbed BA homeostasis and decreased C4 levels in *Lgr4/5dLKO* mice, with the latter implying altered cholesterol metabolism that led to a minor

compensatory increase in VLDL cholesterol content in serum. This is in agreement with the decreased expression of *Cyp27a1*, an enzyme involved in the catabolism of cholesterol towards BAs, both via the alternative and the classical BA biosynthesis pathway, detected in 3-month-old Lgr4/5dLKO mice. Despite hepatic steatosis, these animals maintained normal body weight. On HFD challenge, Lgr4/5dLKO mice developed liver inflammation and fibrosis, and serum contained elevated aspartate aminotransferase and alanine aminotransferase levels.

In summary, these data show how loss of metabolic zonation on hepatic epithelial cell-specific *Lgr4/5* ablation led to multiple molecular alterations that predisposed livers to steatosis and NAFLD progression. These events were manifested by transcriptional and lipid changes in the liver affecting not only hepatocyte physiology but also inflammation and hepatic stellate cell activation. Insights into this complex interaction network will likely result in the formation of new therapeutic hypotheses for the treatment of NAFLD.

## Acknowledgments

We thank Ryan Streeper, Ludovic Perrot, Sabrina Silvia Surber, Nathalie Stuber, Martin van de Velde, Gabi Schutzius, Adrian Salathe, Berangere Gapp, Benjamin Kueng, Pauline Fernandez, and Dominic Trojer for technical assistance; and Klaus Seuwen, Susan Kirkland, Gabriele Hintzen, Felix Lohmann, and Anne Granger for helpful discussion and critical reading of the manuscript.

## Author Contributions

E.S. and H.R. conceived the study; E.S., C.P., V.O., A.F., A.A., M.L.M.-G., V.B., B.F., P.O., J.T., A.G.M., L.B., G.d'A., W.C., S.A., M.O., N.B., C.S., and S.L. performed the experiments; E.S., H.R., T.B., J.S.T., C.P., M.B., S.M.R., I.K., F.N., L.M.T., Z.-Y.W., and H.S.S. discussed and interpreted results; A.O., M.B., G.R., P.T., N.B., C.S., I.K., C.G., and J.S.T. provided the key materials and instructions for use; E.S. and H.R. wrote the manuscript; and H.R. and T.B. supervised the project.

## Supplemental Data

Supplemental material for this article can be found at <http://doi.org/10.1016/j.ajpath.2022.10.008>.

## References

- Ben-Moshe S, Itzkovitz S: Spatial heterogeneity in the mammalian liver. *Nat Rev Gastroenterol Hepatol* 2019, 16:395–410
- Gebhardt R: Metabolic zonation of the liver: regulation and implications for liver function. *Pharmacol Ther* 1992, 53:275–354

- Peng K, Mo Z, Tian G: Serum lipid abnormalities and nonalcoholic fatty liver disease in adult males. *Am J Med Sci* 2017, 353:236–241
- Bashiri A, Tavallae G, Li LX, Ng DS: Emerging role of cellular cholesterol in the pathogenesis of nonalcoholic fatty liver disease. *Curr Opin Lipidol* 2013, 24:275–276
- Musso G, Gambino R, Cassader M: Cholesterol metabolism and the pathogenesis of non-alcoholic steatohepatitis. *Prog Lipid Res* 2013, 52:175–191
- Behari J: The Wnt/beta-catenin signaling pathway in liver biology and disease. *Expert Rev Gastroenterol Hepatol* 2010, 4:745–756
- Lemberger UJ, Fuchs CD, Karer M, Haas S, Stojakovic T, Schofer C, Marschall HU, Wrba F, Taketo MM, Egger G, Trauner M, Osterreicher CH: Hepatocyte specific expression of an oncogenic variant of beta-catenin results in cholestatic liver disease. *Oncotarget* 2016, 7:86985–86998
- Matsumoto K, Imasato M, Yamazaki Y, Tanaka H, Watanabe M, Eguchi H, Nagano H, Hikita H, Tatsumi T, Takehara T, Tamura A, Tsukita S: Claudin 2 deficiency reduces bile flow and increases susceptibility to cholesterol gallstone disease in mice. *Gastroenterology* 2014, 147:1134–1145.e10
- Son S, Kojima T, Decaens C, Yamaguchi H, Ito T, Imamura M, Murata M, Tanaka S, Chiba H, Hirata K, Sawada N: Knockdown of tight junction protein claudin-2 prevents bile canalicular formation in WIF-B9 cells. *Histochem Cell Biol* 2009, 131:411–424
- MacDonald BT, Tamai K, He X: Wnt/beta-catenin signaling: components, mechanisms, and diseases. *Dev Cell* 2009, 17:9–26
- Russell JO, Monga SP: Wnt/beta-catenin signaling in liver development, homeostasis, and pathobiology. *Annu Rev Pathol* 2018, 13:351–378
- Benhamouche S, Decaens T, Godard C, Chambrey R, Rickman DS, Moinard C, Vasseur-Cognet M, Kuo CJ, Kahn A, Perret C, Colnot S: Apc tumor suppressor gene is the “zonation-keeper” of mouse liver. *Dev Cell* 2006, 10:759–770
- Ma R, Martinez-Ramirez AS, Borders TL, Gao F, Sosa-Pineda B: Metabolic and non-metabolic liver zonation is established non-synchronously and requires sinusoidal Wnts. *Elife* 2020, 9:e46206
- Yang J, Mowry LE, Nejak-Bowen KN, Okabe H, Diegel CR, Lang RA, Williams BO, Monga SP: beta-Catenin signaling in murine liver zonation and regeneration: a Wnt-Wnt situation! *Hepatology* 2014, 60:964–976
- de Lau W, Barker N, Low TY, Koo BK, Li VS, Teunissen H, Kujala P, Haegebarth A, Peters PJ, van de Wetering M, Stange DE, van Es JE, Guardavaccaro D, Schasfoort RB, Mohri Y, Nishimori K, Mohammed S, Heck AJ, Clevers H: Lgr5 homologues associate with Wnt receptors and mediate R-spondin signalling. *Nature* 2011, 476:293–297
- Hao HX, Xie Y, Zhang Y, Charlat O, Oster E, Avello M, Lei H, Mickanin C, Liu D, Ruffner H, Mao X, Ma Q, Zamponi R, Bouwmeester T, Finan PM, Kirschner MW, Porter JA, Serluca FC, Cong F: ZNRF3 promotes Wnt receptor turnover in an R-spondin-sensitive manner. *Nature* 2012, 485:195–200
- Koo BK, Spit M, Jordens I, Low TY, Stange DE, van de Wetering M, van Es JH, Mohammed S, Heck AJ, Maurice MM, Clevers H: Tumour suppressor RNF43 is a stem-cell E3 ligase that induces endocytosis of Wnt receptors. *Nature* 2012, 488:665–669
- Ruffner H, Sprunger J, Charlat O, Leighton-Davies J, Grosshans B, Salathe A, Zietzling S, Beck V, Therier M, Isken A, Xie Y, Zhang Y, Hao H, Shi X, Liu D, Song Q, Clay I, Hintzen G, Tchorz J, Bouchez LC, Michaud G, Finan P, Myer VE, Bouwmeester T, Porter J, Hild M, Bassilana F, Parker CN, Cong F: R-Spondin potentiates Wnt/beta-catenin signaling through orphan receptors LGR4 and LGR5. *PLoS One* 2012, 7:e40976
- Planas-Paz L, Sun T, Pikiolok M, Cochran NR, Bergling S, Orsini V, et al: YAP, but not RSPO-LGR4/5, signaling in biliary epithelial cells promotes a ductular reaction in response to liver injury. *Cell Stem Cell* 2019, 25:39–53.e10

20. Planas-Paz L, Orsini V, Boulter L, Calabrese D, Pikiolek M, Nigsch F, Xie Y, Roma G, Donovan A, Marti P, Beckmann N, Dill MT, Carbone W, Bergling S, Isken A, Mueller M, Kinzel B, Yang Y, Mao X, Nicholson TB, Zamponi R, Capodiceci P, Valdez R, Rivera D, Loew A, Ukomadu C, Terracciano LM, Bouwmeester T, Cong F, Heim MH, Forbes SJ, Ruffner H, Tchorz JS: The RSPO-LGR4/5-ZNRF3/RNF43 module controls liver zonation and size. *Nat Cell Biol* 2016, 18:467–479
21. Belenguer G, Mastrogianni G, Pacini C, Hall Z, Dowbaj AM, Arnes-Benito R, Sljukic A, Prior N, Kakava S, Bradshaw CR, Davies S, Vacca M, Saeb-Parsy K, Koo BK, Huch M: RNF43/ZNRF3 loss predisposes to hepatocellular-carcinoma by impairing liver regeneration and altering the liver lipid metabolic ground-state. *Nat Commun* 2022, 13:334
22. Behari J, Li HN, Liu SG, Stefanovic-Racic M, Alonso L, O'Donnell CP, Shiva S, Singamsetty S, Watanabe Y, Singh VP, Liu Q: beta-Catenin links hepatic metabolic zonation with lipid metabolism and diet-induced obesity in mice. *Am J Pathol* 2014, 184:3284–3298
23. Sun T, Annunziato S, Bergling S, Sheng C, Orsini V, Forcella P, Pikiolek M, Kancherla V, Holwerda S, Imanci D, Wu F, Meylan LC, Puehringer LF, Waldt A, Oertli M, Schuierer S, Terracciano LM, Reinker S, Ruffner H, Bouwmeester T, Sailer AW, George E, Roma G, de Weck A, Piscuoglio S, Lohmann F, Naumann U, Liberali P, Cong F, Tchorz JS: ZNRF3 and RNF43 cooperate to safeguard metabolic liver zonation and hepatocyte proliferation. *Cell Stem Cell* 2021, 28:1822–1837.e10
24. Behari J, Yeh TH, Krauland L, Otruba W, Ciepły B, Hauth B, Apte U, Wu T, Evans R, Monga SPS: Liver-specific beta-catenin knockout mice exhibit defective bile acid and cholesterol homeostasis and increased susceptibility to diet-induced steatohepatitis. *Am J Pathol* 2010, 176:744–753
25. Go GW, Srivastava R, Hernandez-Ono A, Gang G, Smith SB, Booth CJ, Ginsberg HN, Mani A: The combined hyperlipidemia caused by impaired Wnt-LRP6 signaling is reversed by Wnt3a rescue. *Cell Metab* 2014, 19:209–220
26. Saponara E, Penno C, Matadamas-Guzmán ML, Brun V, Fischer B, Brousseau M, Wang ZY, O'Donnell P, Turner J, Graff Meyer A, Bollepalli L, d'Ario G, Roma G, Carbone W, Orsini V, Annunziato S, Obrecht M, Beckmann N, Saravanan C, Osmont A, Tropberger P, Richards S, Genoud C, Aebi A, Ley S, Ksiazek I, Nigsch F, Terracciano L, Bouwmeester T, Tchorz JS, Ruffner H: Loss of hepatic *Lgr4* and *Lgr5* promotes nonalcoholic fatty liver disease. *bioRxiv* 2021, [Preprint] doi: 10.1101/2021.11.22.469602
27. McGuinness OP, Ayala JE, Laughlin MR, Wasserman DH: NIH experiment in centralized mouse phenotyping: the Vanderbilt experience and recommendations for evaluating glucose homeostasis in the mouse. *Am J Physiol Endocrinol Metab* 2009, 297:E849–E855
28. Yu G, Wang LG, Han Y, He QY: clusterProfiler: an R package for comparing biological themes among gene clusters. *OMICS* 2012, 16:284–287
29. Yu G, He QY: ReactomePA: an R/Bioconductor package for reactome pathway analysis and visualization. *Mol Biosyst* 2016, 12:477–479
30. Aibar S, Gonzalez-Blas CB, Moerman T, Huynh-Thu VA, Imrichova H, Hulsemans G, Rambow F, Marine JC, Geurts P, Aerts J, van den Oord J, Atak ZK, Wouters J, Aerts S: SCENIC: single-cell regulatory network inference and clustering. *Nat Methods* 2017, 14:1083–1086
31. Schadt HS, Wolf A, Mahl JA, Wuersch K, Couttet P, Schwald M, Fischer A, Lienard M, Emotte C, Teng CH, Skuba E, Richardson TA, Manenti L, Weiss A, Graus Porta D, Fairhurst RA, Kullak-Ublick GA, Chibout SD, Pognan F, Kluge W, Kinyamu-Akunda J: Bile acid sequestration by cholestyramine mitigates FGFR4 inhibition-induced ALT elevation. *Toxicol Sci* 2018, 163:265–278
32. Tsugawa H, Ikeda K, Takahashi M, Satoh A, Mori Y, Uchino H, Okahashi N, Yamada Y, Tada I, Bonini P, Higashi Y, Okazaki Y, Zhou Z, Zhu ZJ, Koelmel J, Cajka T, Fiehn O, Saito K, Arita M, Arita M: A lipidome atlas in MS-DIAL 4. *Nat Biotechnol* 2020, 38:1159–1163
33. De Livera AM, Olshansky G, Simpson JA, Creek DJ: NormalizedMets: assessing, selecting and implementing statistical methods for normalizing metabolomics data. *Metabolomics* 2018, 14:54
34. De Livera AM, Sysi-Aho M, Jacob L, Gagnon-Bartsch JA, Castillo S, Simpson JA, Speed TP: Statistical methods for handling unwanted variation in metabolomics data. *Anal Chem* 2015, 87:3606–3615
35. Gapp B, Jourdain M, Bringer P, Kueng B, Weber D, Osmont A, Zurbrugg S, Knehr J, Falchetto R, Roma G, Dietrich W, Valdez R, Beckmann N, Nigsch F, Sanyal AJ, Ksiazek I: Farnesoid X receptor agonism, acetyl-coenzyme A carboxylase inhibition, and back translation of clinically observed endpoints of de novo lipogenesis in a murine NASH model. *Hepato Comm* 2020, 4:109–125
36. Chatrath H, Vuppalanchi R, Chalasani N: Dyslipidemia in patients with nonalcoholic fatty liver disease. *Semin Liver Dis* 2012, 32:22–29
37. Millar JS, Cromley DA, McCoy MG, Rader DJ, Billheimer JT: Determining hepatic triglyceride production in mice: comparison of poloxamer 407 with Triton WR-1339. *J Lipid Res* 2005, 46:2023–2028
38. Quinn WJ 3rd, Wan M, Shewale SV, Gelfer R, Rader DJ, Birnbaum MJ, Titchenell PM: mTORC1 stimulates phosphatidylcholine synthesis to promote triglyceride secretion. *J Clin Invest* 2017, 127:4207–4215
39. Fabbrini E, Mohammed BS, Magkos F, Korenblat KM, Patterson BW, Klein S: Alterations in adipose tissue and hepatic lipid kinetics in obese men and women with nonalcoholic fatty liver disease. *Gastroenterology* 2008, 134:424–431
40. Zhu L, Luu T, Emfinger CH, Parks BA, Shi J, Trefts E, Zeng F, Kuklenyik Z, Harris RC, Wasserman DH, Fazio S, Stafford JM: CETP inhibition improves HDL function but leads to fatty liver and insulin resistance in CETP-expressing transgenic mice on a high-fat diet. *Diabetes* 2018, 67:2494–2506
41. Mashek DG: Hepatic fatty acid trafficking: multiple forks in the road. *Adv Nutr* 2013, 4:697–710
42. Griffett K, Bedia-Diaz G, Elgendy B, Burris TP: REV-ERB agonism improves liver pathology in a mouse model of NASH. *PLoS One* 2020, 15:e0236000
43. Norton L, Chen X, Fourcaudot M, Acharya NK, DeFronzo RA, Heikkinen S: The mechanisms of genome-wide target gene regulation by TCF7L2 in liver cells. *Nucleic Acids Res* 2014, 42:13646–13661
44. Qiu B, Simon MC: BODIPY 493/503 staining of neutral lipid droplets for microscopy and quantification by flow cytometry. *Bio Protoc* 2016, 6:e1912
45. Germano D, Uteng M, Pognan F, Chibout SD, Wolf A: Determination of liver specific toxicities in rat hepatocytes by high content imaging during 2-week multiple treatment. *Toxicol In Vitro* 2015, 30:79–94
46. de Waart DR, Hausler S, Vlaming ML, Kunne C, Hanggi E, Gruss HJ, Oude Elferink RP, Stieger B: Hepatic transport mechanisms of cholestyramine-L-lysyl-fluorescein. *J Pharmacol Exp Ther* 2010, 334:78–86
47. Fickert P, Wagner M: Biliary bile acids in hepatobiliary injury - what is the link? *J Hepatol* 2017, 67:619–631
48. Pradhan-Sundt T, Monga SP: Blood-bile barrier: morphology, regulation, and pathophysiology. *Gene Expr* 2019, 19:69–87
49. Galman C, Arvidsson I, Angelin B, Rudling M: Monitoring hepatic cholesterol 7alpha-hydroxylase activity by assay of the stable bile acid intermediate 7alpha-hydroxy-4-cholesten-3-one in peripheral blood. *J Lipid Res* 2003, 44:859–866
50. Csanaky IL, Lu H, Zhang Y, Ogura K, Choudhuri S, Klaassen CD: Organic anion-transporting polypeptide 1b2 (Oatp1b2) is important for the hepatic uptake of unconjugated bile acids: studies in Oatp1b2-null mice. *Hepatology* 2011, 53:272–281
51. Mahagita C, Grassl SM, Piyachaturawat P, Ballatori N: Human organic anion transporter 1B1 and 1B3 function as bidirectional

- carriers and do not mediate GSH-bile acid cotransport. *Am J Physiol Gastrointest Liver Physiol* 2007, 293:G271–G278
52. Lorbek G, Lewinska M, Rozman D: Cytochrome P450s in the synthesis of cholesterol and bile acids—from mouse models to human diseases. *FEBS J* 2012, 279:1516–1533
  53. Uno S, Nebert DW, Makishima M: Cytochrome P450 1A1 (CYP1A1) protects against nonalcoholic fatty liver disease caused by Western diet containing benzo[a]pyrene in mice. *Food Chem Toxicol* 2018, 113:73–82
  54. Alves-Bezerra M, Cohen DE: Triglyceride metabolism in the liver. *Compr Physiol* 2017, 8:1–8
  55. Brejchova K, Radner FPW, Balas L, Paluchova V, Cajka T, Chodounska H, Kudova E, Schratte M, Schreiber R, Durand T, Zechner R, Kuda O: Distinct roles of adipose triglyceride lipase and hormone-sensitive lipase in the catabolism of triacylglycerol estolides. *Proc Natl Acad Sci U S A* 2021, 118. e2020999118
  56. Riecan M, Paluchova V, Lopes M, Brejchova K, Kuda O: Branched and linear fatty acid esters of hydroxy fatty acids (FAHFA) relevant to human health. *Pharmacol Ther* 2022, 231:107972
  57. Ramachandran P, Dobie R, Wilson-Kanamori JR, Dora EF, Henderson BEP, Luu NT, Portman JR, Matchett KP, Brice M, Marwick JA, Taylor RS, Eftremova M, Vento-Tormo R, Carragher NO, Kendall TJ, Fallowfield JA, Harrison EM, Mole DJ, Wigmore SJ, Newsome PN, Weston CJ, Iredale JP, Tacke F, Pollard JW, Ponting CP, Marioni JC, Teichmann SA, Henderson NC: Resolving the fibrotic niche of human liver cirrhosis at single-cell level. *Nature* 2019, 575:512–518
  58. Wang ZY, Keogh A, Waldt A, Cuttar R, Neri M, Zhu S, Schuierer S, Ruchti A, Crochemore C, Knehr J, Bastien J, Ksiazek I, Sanchez-Taltavull D, Ge H, Wu J, Roma G, Helliwell SB, Stroka D, Nigsch F: Single-cell and bulk transcriptomics of the liver reveals potential targets of NASH with fibrosis. *Sci Rep* 2021, 11:19396
  59. Gerbal-Chaloin S, Dume AS, Briolotti P, Klieber S, Raullet E, Duret C, Fabre JM, Ramos J, Maurel P, Daujat-Chavanieu M: The WNT/beta-catenin pathway is a transcriptional regulator of CYP2E1, CYP1A2, and aryl hydrocarbon receptor gene expression in primary human hepatocytes. *Mol Pharmacol* 2014, 86: 624–634
  60. Annunziato S, Sun T, Tchorz JS: The RSPO-LGR4/5-ZNRF3/RNF43 module in liver homeostasis, regeneration, and disease. *Hepatology* 2022, 76:888–899
  61. Mani A, Radhakrishnan J, Wang H, Mani A, Mani MA, Nelson-Williams C, Carew KS, Mane S, Najmabadi H, Wu D, Lifton RP: LRP6 mutation in a family with early coronary disease and metabolic risk factors. *Science* 2007, 315:1278–1282
  62. Wang J, Liu R, Wang F, Hong J, Li X, Chen M, Ke Y, Zhang X, Ma Q, Wang R, Shi J, Cui B, Gu W, Zhang Y, Zhang Z, Wang W, Xia X, Liu M, Ning G: Ablation of LGR4 promotes energy expenditure by driving white-to-brown fat switch. *Nat Cell Biol* 2013, 15:1455–1463
  63. Wang F, Zhang XF, Wang JQ, Chen MP, Fan NG, Ma QY, Liu RX, Wang R, Li XY, Liu MY, Ning G: LGR4 acts as a link between the peripheral circadian clock and lipid metabolism in liver. *J Mol Endocrinol* 2014, 52:133–143
  64. Campbell HK, Maier JL, DeMali KA: Interplay between tight junctions & adherens junctions. *Exp Cell Res* 2017, 358:39–44
  65. Chalasani N, Wilson L, Kleiner DE, Cummings OW, Brunt EM, Unalp A, Network NCR: Relationship of steatosis grade and zonal location to histological features of steatohepatitis in adult patients with non-alcoholic fatty liver disease. *J Hepatol* 2008, 48:829–834
  66. Straub BK, Stoeffel P, Heid H, Zimbelmann R, Schirmacher P: Differential pattern of lipid droplet-associated proteins and de novo perilipin expression in hepatocyte steatogenesis. *Hepatology* 2008, 47:1936–1946
  67. Hall Z, Bond NJ, Ashmore T, Sanders F, Ament Z, Wang XZ, Murray AJ, Bellafante E, Virtue S, Vidal-Puig A, Allison M, Davies SE, Koulman A, Vacca M, Griffin JL: Lipid zonation and phospholipid remodeling in nonalcoholic fatty liver disease. *Hepatology* 2017, 65:1165–1180
  68. Yang L, Wang J, Gong X, Fan Q, Yang X, Cui Y, Gao X, Li L, Sun X, Li Y, Wang Y: Emerging roles for LGR4 in organ development, energy metabolism and carcinogenesis. *Front Genet* 2021, 12: 728827
  69. Li B, Yao Q, Guo S, Ma S, Dong Y, Xin H, Wang H, Liu L, Chang W, Zhang Y: Type 2 diabetes with hypertensive patients results in changes to features of adipocytokines: leptin, Irisin, LGR4, and Sfrp5. *Clin Exp Hypertens* 2019, 41:645–650
  70. Zou Y, Ning T, Shi J, Chen M, Ding L, Huang Y, Kauderer S, Xu M, Cui B, Bi Y, Liu S, Hong J, Liu R, Ning G, Wang J: Association of a gain-of-function variant in LGR4 with central obesity. *Obesity (Silver Spring)* 2017, 25:252–260
  71. Chen Z, Yu H, Shi X, Warren CR, Lotta LA, Friesen M, Meissner TB, Langenberg C, Wabitsch M, Wareham N, Benson MD, Gerszten RE, Cowan CA: Functional screening of candidate causal genes for insulin resistance in human preadipocytes and adipocytes. *Circ Res* 2020, 126:330–346
  72. Heid IM, Jackson AU, Randall JC, Winkler TW, Qi L, Steinthorsdottir V, et al: Meta-analysis identifies 13 new loci associated with waist-hip ratio and reveals sexual dimorphism in the genetic basis of fat distribution. *Nat Genet* 2010, 42:949–960
  73. Bhatt HB, Smith RJ: Fatty liver disease in diabetes mellitus. *HepatoBiliary Surg Nutr* 2015, 4:101–108
  74. Clarke JD, Novak P, Lake AD, Shipkova P, Aranibar N, Robertson D, Severson PL, Reily MD, Futscher BW, Lehman-McKeeman LD, Cherrington NJ: Characterization of hepatocellular carcinoma related genes and metabolites in human nonalcoholic fatty liver disease. *Dig Dis Sci* 2014, 59:365–374
  75. Xie Y, Tian H, Xiang B, Li D, Liu J, Cai Z, Liu Y, Xiang H: Total polyunsaturated fatty acid intake and the risk of non-alcoholic fatty liver disease in Chinese Han adults: a secondary analysis based on a case-control study. *BMC Gastroenterol* 2021, 21:451
  76. Yeh TH, Krauland L, Singh V, Zou BB, Devaraj P, Stolz DB, Franks J, Monga SPS, Sasatomi E, Behari J: Liver-specific beta-catenin knockout mice have bile canalicular abnormalities, bile secretory defect, and intrahepatic cholestasis. *Hepatology* 2010, 52: 1410–1419
  77. Pradhan-Sundt T, Liu S, Singh S, Poddar M, Ko S, Bell A, Franks J, Huck I, Stolz D, Apte U, Ranganathan S, Nejak-Bowen K, Monga SP: Dual beta-catenin and gamma-catenin loss in hepatocytes impacts their polarity through altered transforming growth factor-beta and hepatocyte nuclear factor 4alpha signaling. *Am J Pathol* 2021, 191:885–901
  78. Trauner M, Fuchs CD: Novel therapeutic targets for cholestatic and fatty liver disease. *Gut* 2022, 71:194–209
  79. Dongiovanni P, Petta S, Maglio C, Fracanzani AL, Pipitone R, Mozzi E, Motta BM, Kaminska D, Rametta R, Grimaudo S, Pelusi S, Montalcini T, Alisi A, Maggioni M, Karja V, Boren J, Kakela P, Di Marco V, Xing C, Nobili V, Dallapiccola B, Craxi A, Pihlajamaki J, Fargion S, Sjostrom L, Carlsson LM, Romeo S, Valenti L: Transmembrane 6 superfamily member 2 gene variant disentangles nonalcoholic steatohepatitis from cardiovascular disease. *Hepatology* 2015, 61:506–514
  80. Fabbri E, Magkos F: Hepatic steatosis as a marker of metabolic dysfunction. *Nutrients* 2015, 7:4995–5019
  81. Lee K, Shin Y, Cheng R, Park K, Hu Y, McBride J, He XM, Takahashi Y, Ma JX: Receptor heterodimerization as a novel mechanism for the regulation of Wnt/beta-catenin signaling. *J Cell Sci* 2014, 127:4857–4869